



Pulse-Cavitation Vibrating Drilling Prototype Development and Evaluation

by

© Oleksii Pronin

A Thesis submitted to the

School of Graduate Studies

in partial fulfillment of the requirements for the degree of

Master of Engineering

Faculty of Engineering and Applied Science

Memorial University of Newfoundland

July, 2012

St. John's, Newfoundland, Canada

ABSTRACT

The drilling rate decreases with an increase in depth due to high pressure at the bottom hole. Accordingly, there is a need for an improved rock penetration mechanism to increase the drilling speed in deep drilling conditions. Historically, vibration assisted drilling has shown the ability to improve the penetration rate. Therefore, current research aims to develop a vibrating tool to be used for experimental investigation in the laboratory and in the field.

Considering existing vibration and pressure pulsation tools, a pulse-cavitation vibrating prototype was proposed. The vibrating tool, suggested for drilling penetration improvement, was proposed to be installed behind the bit as a drill collar sub. It should operate in deep drilling conditions and produce two major effects: high amplitude and high frequency pressure pulsations and vibrations.

Prototype feasibility was tested using computational fluid dynamics (CFD) analysis. The tool was simulated to examine cavitation initiation and observe pressure pulsation patterns over a pressure range available in the laboratory facilities, and at pressures similar to deep drilling conditions. In addition, the density and viscosity of different drilling fluids on the performance of the prototype were analyzed. The prototype pulse-cavitation tool was manufactured and tested in laboratory facilities. A series of experiments was performed to obtain a significant tool operation experience. Measurements of pressure pulsations along with vibration accelerations were obtained during these experiments. Data yielded agreement of these parameters, therefore, it was

concluded that cavitation produced the high frequency pressure pulsations, which caused vibration accelerations on the prototype.

Initial CFD and experimental results show promise for the pulse cavitation tool use in creating high frequency pressure pulses and vibrations. The prototype can now be used for further performance and vibration assisted drilling investigations. The experience gained in the experimental operation provides a background for future prototype improvement and development.

ACKNOWLEDGEMENTS

I would like to express my genuine gratitude to my academic supervisor Professor Stephen Butt for funding my research, providing me with guidance in experimental work and thesis preparation, great training, courses and other experiences that I have gained while studying at Memorial University of Newfoundland.

I would also like to thank Project Managers and Engineers, Farid Arvani, Heng Li and Brock Gillis, for their assistance with various technical issues, equipment ordering and useful suggestions and comments regarding the project.

I wish to thank all current and previous members of the Advanced Drilling Group for their cooperation, support and friendly environment. Special thanks to Hossein Khorshidian for assistance with drawings, and Sadegh Babapour, Yousef Gharibiyamchi, Pushpinder Singh Rana, Mohammad Mozaffari and Qian Gao for assistance with experiments and data analysis.

I wish to thank the Technical Services personnel, David Snook and Ron Monks, for all manufactured tools and parts, technical help, advice and assistance.

Finally, I want to thank my family and friends for their support, motivation and inspiration in my studies.

This research was conducted at the Advanced Drilling Technology Laboratory at Memorial University of Newfoundland and was funded by the Atlantic Canada Opportunities Agency (AIF Contract no. 781-2636-1920044), the Research and Development Corporation of Newfoundland and Labrador, Husky Energy, and Suncor Energy.

Table of Contents

ABSTRACT	ii
ACKNOWLEDGEMENTS	iv
Table of Contents	v
List of Tables.....	viii
List of Figures	ix
List of Symbols, Nomenclature or Abbreviations.....	xiii
Note on Units	xv
List of Appendices	xvi
1 Introduction.....	1
1.1 Introduction	1
1.2 Research Scope and Objectives.....	4
1.3 Research Background.....	5
1.4 Significance of the Research	10
2 Literature Review	12
2.1 Existing Down-Hole Drilling Tools.....	12
2.1.1 Novatek Mud Hammer.....	12
2.1.2 Tempress Tool.....	15
2.1.3 Hydraulic Pulsed Cavitating Tool	17
2.1.4 Agitator Tool	18

2.1.5	Hydraulic Jar	20
2.1.6	High Frequency Cavitation Hydrovibrator.....	22
2.2	Cavitation Theory.....	23
3	Cavitation Drilling Tool Concept Description	35
4	Prototype CFD Simulations.....	52
4.1	Confirmation of Tool Operation within Experimental Capabilities.....	54
4.2	High Pressure Simulations	62
4.3	Estimation of Density and Viscosity Influence on Tool Performance.....	69
4.4	Simulation Conclusions.....	76
5	Prototype Development	79
5.1	Prototype Orifice Size Consideration.....	79
5.2	Pulse-Cavitation Prototype Design	85
5.3	Experimental Setup	90
6	Prototype Experiments.....	93
6.1	Initial Experimental Observations.....	93
6.2	Characterization Tests	95
6.3	Prototype Performance Evaluation Experiments	100
6.4	Confirmation Tests.....	127
7	Conclusions and Future Work	137
7.1	Conclusions	137
7.2	Future Work	140

Appendix A: Downhole vibration tools specifications	147
Appendix B: Prototype Drawings	148
Appendix C: Experimental Results	151
Appendix D: Confirmation Test Results.....	154

List of Tables

Table 3.1 – Pulsation frequency at diffuser angle 15° and inlet pressure 725 psig [17]	37
Table 3.2 – Proposed operational conditions for hydrovibrator [17]	38
Table 3.3 – Components of the ITM hydraulic system	42
Table 3.4 – Hydrovibrator performance characteristics [18]	50
Table 3.5 – Operational parameters for hydrovibrators of different orifice size [19]	50
Table 4.1 – Constant inlet parameters for simulations	55
Table 4.2 – First simulations variable input parameters	55
Table 4.3 – Output parameters of the first simulations	57
Table 4.4 – First simulation results	61
Table 4.5 – Constant inlet factors for high pressure simulations	63
Table 4.6 – High pressure simulation variable input parameters	64
Table 4.7 – Output parameters of high pressure simulations	64
Table 4.8 – Variable factors for density and viscosity simulation investigation	71
Table 5.1 – Flow rate boundaries for different nozzle sizes	80
Table 5.2 – Pressure loss across the orifice calculated by first method	82
Table 5.3 – Pressure drop calculation by second method	83
Table 5.4 - Flow rate that will produce 800 psi pressure drop across the orifice	85
Table 5.5 – Pump specifications	90
Table 6.1 – Data obtained downstream of the 5 foot pipe	97
Table 6.2 – Data obtained directly downstream of the prototype	98

List of Figures

Figure 1.1 – Penetration rate as a function of pressure [3]	3
Figure 1.2 – Experimental results of vibration application during core drilling [5]	6
Figure 1.3 – ROP versus vibration amplitude [5]	7
Figure 1.4 – Experimental results with the full face bit [6]	7
Figure 2.1 – Novatek mud hammer [9]	13
Figure 2.2 – Hydraulic pulse drilling tool [10]	16
Figure 2.3 - Hydraulic pulsed cavitating jet generator [13]	17
Figure 2.4 – Agitator tool [14]	19
Figure 2.5 – Typical jar schematic diagram [15]	21
Figure 2.6 - High-frequency cavitation hydro-vibrator [18]	22
Figure 2.7 – Diagram of the experimental assembly [22]	25
Figure 2.8 – Peak force of the cavity collapse versus its lifetime. Data presented for ½ inch bar (blank circles) and ¼ inch bar (shaded circles) [22]	26
Figure 2.9 – Collapse and rebound of a cavity of lifetime 800 μ s obtained by streak schlieren photograph [22]	27
Figure 2.10 –Growth and collapse of a cavity with lifetime of 800 μ s obtained by streak schlieren photograph [22]	28
Figure 2.11 – Illustration of cavitation flare [20]	30
Figure 2.12 – Cavitation threshold as a function of frequency [26]	32
Figure 2.13 – Behaviour of a cavity as a function of its radius at constant frequency of 10 kHz and pressures of 10^5 Pa (line 1), $5 \cdot 10^5$ Pa (line 2) and 10^6 Pa (line 3) [26]	33

Figure 3.1 – Peak-to-peak amplitude of p2 versus d2/do [17].....	39
Figure 3.2 – Peak-to-peak amplitude of p2 versus l2/do [17].....	40
Figure 3.3 – Structural layout of the prototype hydrovibrator [17]	41
Figure 3.4 – Hydraulic facilities for the prototype testing at ITM [17]	42
Figure 3.5 – Pressure oscillations at the outlet of the cavitator [17].....	43
Figure 3.6 – Frequency of cavitation oscillations [17, 18].....	44
Figure 3.7- Peak-to-peak amplitude of cavitation oscillations [17, 18].....	45
Figure 3.8 – Time oscillogram of the hydrovibrator vibration accelerations: a1 – upstream of the tool; a2 - on the hydrovibrator; a3 – downstream of the tool [17, 18].....	46
Figure 3.9 – Structural layout of the hydrovibrator prototype [18]	48
Figure 3.10 – Calculated time dependence of the tool parameters: (a) time dependence of the displacement, (b) vibration accelerations, (c) the volume of the cavity [18].....	49
Figure 3.11 – Tools performance curves for inlet pressure 740 psi (left side), inlet pressure 1460 psi (right side) [19].....	51
Figure 4.1 – CFD simulation model.....	53
Figure 4.2 – Simulation results: (a) animation, (b) FFT plot, (c) pressure profile.....	60
Figure 4.3 – Screenshot from DOE software data input	65
Figure 4.4 – Dominant frequency response surface.....	66
Figure 4.5 – Outlet pressure pulses	67
Figure 4.6 – Maximum pressure peak response surface	68
Figure 4.7 – Multiple frequency response surface	69
Figure 4.8 – Screenshot from DOE input for density and viscosity investigation.....	72

Figure 4.9 – Dominant frequency response	73
Figure 4.10 – Maximum pressure peak plot.....	74
Figure 4.11 – Viscosity versus shear rate [34].....	75
Figure 4.12 – Flow 3D fluid database screenshot	76
Figure 5.1 – Schematic view of the prototype design	87
Figure 5.2 – Manufactured pulse-cavitation prototype	89
Figure 5.3 – Labview interface for the prototype experiments	92
Figure 6.1 – Pressure pulses recorded directly downstream of the prototype.....	99
Figure 6.2 – Experimental setup: (a) overall view, (b) inlet, (c) outlet.....	103
Figure 6.3 – Inlet pressure versus flow rate: (a) P vs. Q, (b) P vs. Q^2	107
Figure 6.4 – Pressure pulsations for test run #11	108
Figure 6.5 - Pressure pulsations for test run #46.....	109
Figure 6.6 - Pressure pulsations for test run #48.....	110
Figure 6.7 – Vibration acceleration plot for test run #46	111
Figure 6.8 – FFT plots of amplitude and power spectrum for inlet pressure pulsations: (a) run #15, (b) run #27, (c) run #40.....	114
Figure 6.9 – FFT plots of amplitude and power spectrum for acceleration vibrations: (a) run #4, (b) run #35, (c) run #46	117
Figure 6.10 – FFT plot of amplitude and power spectrum for outlet pressure (test run #11).....	119
Figure 6.11 – FFT plot for outlet pressure (test run #38): (a) full scale, (b) enlarged peaks	121

Figure 6.12 – Frequency response curves [38]	123
Figure 6.13 – Frequency of (a) pressure pulsations and (b) vibration accelerations.....	125
Figure 6.14 – Vibration frequencies versus inlet pressure	126
Figure 6.15 – Vibration frequency versus P2/P1 ratio	128
Figure 6.16 - Vibration amplitude versus P2/P1 ratio.....	129
Figure 6.17 – Pump pressure pulsations.....	130
Figure 6.18 – FFT description of pressure pulsations caused by: 1- cavitation, 2- pump pulsations, 3 - noise	133
Figure 6.19 – Rust observation on the prototype surfaces: (a) orifice, (b) exterior, (c) inlet	136

List of Symbols, Nomenclature or Abbreviations

ADG	Advanced Drilling Group
API	American Petroleum Institute
CFD	Computational Fluid Dynamics
DAQ	Data Acquisition System
DOE	Design of Experiments
FFT	Fast Fourier Transform
ITM	Institute of Technical Mechanics
NG	Natural Gas
NPT	National Pipe Thread
PDC	Polycrystalline Diamond Compact
ROP	Rate of Penetration
RSM	Response Surface Methodology
S.I.	International System of Units (metric system)
VARD	Vibration Assisted Rotary Drilling
VFD	Variable Frequency Drive
WOB	Weight on Bit
p_1, p_2	Inlet and outlet pressure of the cavitator (Venturi tube)
d_2	Outlet pipe diameter
d_o	Orifice diameter of the tool

τ	Cavitation parameter
m	Mass flow rate through the orifice (converging-diverging passage)
μ	Flow coefficient of the passage
p_k	Pressure in the cavity
ρ	Density of the fluid

Note on Units

Two measurement unit systems were used in this thesis: S.I. and traditional (Imperial and American). In most of the cases traditional units were chosen due to several reasons:

- this study is oriented to the drilling engineering branch of the petroleum industry in North America, where imperial units are more commonly used by the majority of engineers;
- many American Petroleum Institute (API) standards contain non-S.I. units, as well as industrial drilling equipment specifications presented in imperial units, such as drill string components and drill bits;
- the majority of reviewed publications in the drilling engineering field present results in imperial units.

Considering mentioned points, it was decided to give preference to imperial units; however, in some cases S.I. units were used, where this system was more applicable. The table of conversion presents conversion factors for non-S.I. units.

Table of conversion: imperial to metric

Imperial	Multiplying factor	Metric
US gpm	0.0000631	m ³ /s
psi	6895	Pa
in	0.0254	m
feet	0.3048	m
lb (mass)	0.4536	kg

List of Appendices

Appendix A: Downhole vibration tools specifications

Appendix B: Prototype Drawings

Appendix C: Experimental Results

Appendix D: Confirmation Test Results

1 Introduction

1.1 Introduction

Currently, worldwide energy demand continues to increase. According to the latest energy outlook published by British Petroleum (BP), world energy consumption will increase up to 39% in the next 18 years [1]. Hydrocarbon sources of energy, which mainly consist of oil and natural gas (NG), have been predicted to satisfy 54% of the total energy demand by the year 2030. Although market prices for oil and natural gas are increasing, this forecast shows that hydrocarbons will remain the main worldwide energy source for this timeframe. This means that the petroleum industry has to face the challenge in order to discover, produce and deliver the required amount of oil and gas.

Any oil and gas field requires significant investments in order to be discovered and produced. Among the many field development stages, drilling is often the most expensive activity. Its part in overall investment becomes even more significant when drilling takes place offshore, in deep water and in harsh environments. Day rates for jackup rigs (with a water depth of up to 100 m) vary from \$48,000 to \$148,000 USD; floating rigs that are suitable for a harsh environment and deep water depth (up to 3000 m and even more) are more expensive and their day rates vary from \$241,000 to \$458,000 USD [2]. The high cost of rig rentals challenges petroleum companies to increase the speed of drilling operations. Even if a single well could be drilled a few days faster, a significant amount of money could be saved.

Increasing the speed of drilling operations can be subdivided into two tasks. The first one is to decrease non-penetrating time. This time corresponds to bit tripping, casing operation (routine drilling operations) and fishing tools, kick elimination and other accidental operations. Mostly, non-penetrating time can be reduced by means of accurate well design and drilling operation planning. The second task is to increase the speed of actual drilling, called the rate of penetration (ROP), which is measured in distance drilled per unit time (m/hour). ROP can be increased through optimizing the weight on bit (WOB), setting proper drill bit hydraulics, adjusting favourable rotary speed and other conventional optimizations. In addition to these methods, new advanced approaches could be made in order to increase the ROP.

A major challenge that has been faced by drillers is drilling at great depth. It was observed that the ROP decreases with an increase in drilling depth. This phenomenon was described by Garnier and Lingen [3] in 1959. These authors made an approach to investigate the causes of rock drillability reduction at greater depth. They conducted an experimental study on a number of parameters: drilling mud, pore and confining pressure, bit shape and type. As the result, they came to the conclusion that the major factors that influence rock drillability are mud and pore pressure (Figure 1.1). As we can see from Figure 1.1, pressure increase causes reduction of ROP. Mud and pore pressures are related to hydrostatic pressure; consequently, pressure is higher at greater depth.

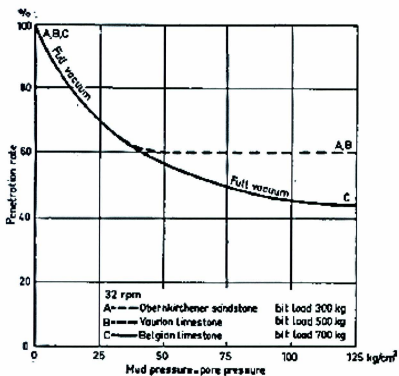


Figure 1.1 – Penetration rate as a function of pressure [3]

It can be concluded that one of the major challenges for current drilling technologies is increasing ROP at depth, as this aspect of drilling becomes very significant, taking into account many deep off- and on-shore hydrocarbon fields.

1.2 Research Scope and Objectives

One of the promising techniques of ROP improvement is vibration drilling, where vibrations are applied to the drilling bit. The advantages of this method were described in earlier publications. A few research studies investigated vibration drilling through experimental work and they showed ROP improvement, especially for hard rocks. One of the major investigations was conducted by an industry consortium in the 1950s, Drilling Investigation Ltd (DRI). Pennington [4] published some of the results of this investigation in 1953. The DRI project was looking into ROP improvement by vibration and percussion drilling. The researchers concluded that drilling can be greatly enhanced by these means, however, they also observed a decrease of the vibration ROP enhancement with depth increase. Eventually, the researchers abandoned the project as they could not reach drilling improvement at depth. Since that time several researchers made an attempt to extend vibration drilling improvement to a greater drilling depth. As a result, a number of approaches were made to develop an efficient drilling vibrating tool, which could be operated during deep drilling. Some promising results were achieved with new downhole tools, however, none of them have become a solution for ROP improvement at great depth. Consequently, it can be concluded that more investigation is required in this field. This means that more experimental studies should be performed, however, there is still a need for an efficient downhole vibration tool, which could eliminate drawbacks of the existing tools. This study aims to develop a prototype that could be used in laboratory and field conditions to conduct drilling experimental investigations.

The vibration tool development was subdivided into a few stages:

- 1) identifying and choosing a promising prototype concept, considering existing downhole vibrating, pulsating and impacting tools;
- 2) simulating potential prototype capabilities within available software packages;
- 3) designing and manufacturing an actual prototype tool, considering the simulation results outcome; and
- 4) prototype performance investigation through experimental analysis.

1.3 Research Background

This study is conducted under the Advanced Exploration Drilling Technology project, which was launched in 2008 at Memorial University of Newfoundland. The main objective of the entire project is to offer a new technology, which is called Vibration-Assisted Rotary Drilling (VARD).

The first investigation of vibration influence on the ROP within the VARD project, was performed by Li [5, 6]. It was proposed that in addition to conventional drilling parameters, vibration on top of the bit could be applied to improve ROP. In order to conduct the investigation a VARD laboratory scale experimental setup was used. This was a modified electrical coring drill rig. During experiments, coring and full face drilling were considered at different levels of rotary speed and vibration amplitude. Vibration frequency was kept constant, as well as a sufficient flow rate for each rotary speed. Experimental results for the coring bit are presented in Figure 1.2. Li suggested that vibration amplitude has a nonlinear relation to ROP and some optimum point might exist.

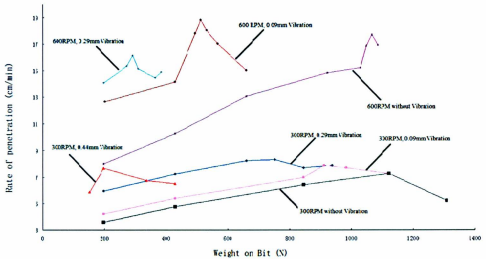


Figure 1.2 – Experimental results of vibration application during core drilling [5]

However, a linear trend of ROP in relation to amplitude was observed during a constant weight on bit (WOB) and constant rotary speed test, as presented in Figure 1.3. The author also concludes from this Figure 1.3, that an ROP increase of more than 100% was obtained with vibration application.

Similar results were obtained during drilling experiments with the full face bit (Figure 1.4). It can be clearly concluded that ROP was enhanced by vibrations.

ROP/Amplitude at 197.6N bit weight, 300 RPM

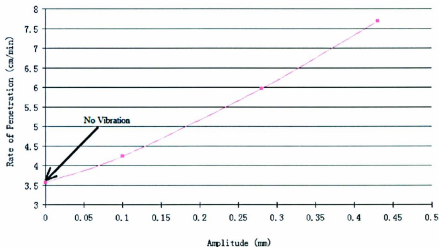


Figure 1.3 – ROP versus vibration amplitude [5]

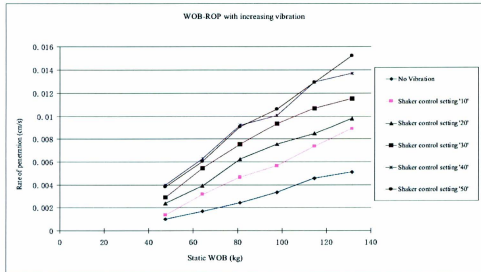


Figure 1.4 – Experimental results with the full face bit [6]

Overall, Li stated a few important conclusions:

- the vibration-assisted technology can significantly increase the ROP;
- as vibration amplitude increases, the founder point of ROP – WOB relation decreases, which means that less WOB can be applied to achieve a higher ROP;
- ROP significantly increases with an increase of vibration amplitude up to the optimum point at constant WOB and rotary speed; and
- vibration amplitude is found to be proportional to the ROP.

The discussed results were encouraging, so the VARD project moved forward to investigate the vibration application for drilling.

Although Li's investigation showed ROP improvement, his tests were conducted at a constant vibration frequency of 60 Hz. The next step of this investigation was conducted by Babatudne [7, 8], who was also a member of the VARD group. Babatunde modified the vibration table that was used for Li's experiments in order to achieve control over the vibration frequency. In addition, the author used diamond drag and polycrystalline diamond compact (PDC) bits for his experimental investigation.

Babatunde considered three levels of amplitude (low, medium and high) and frequency (45, 55 and 65 Hz) for his experiments. First experimental runs were conducted with full face diamond drug bit. Overall, Babatunde recorded ROP improvement (up to more than 100%) at any mode of vibrational drilling[7]. These results brought Babatunde to a few conclusions:

- ROP can be significantly increased with the use of vibrations;
- observed ROP increase range varies from 25% to more than 100%; and
- larger amplitude leads to higher ROP gain.

Another series of experiments was conducted with a PDC bit that has two cutting blades and two nozzles. In agreement with the author's previous results [7], experimental data yielded ROP improvement in all cases of vibration assisted drilling compared to conventional drilling. In addition, the author estimated energy contribution of the drilling experiments and concluded that vibration was a major factor. From this series of experiments Babatunde concluded a few points:

- ROP was improved by vibration while drilling with a PDC bit; and
- optimum frequency of vibration is 65 Hz for lower WOB and 55 Hz for higher WOB.

Another significant observation was that frequency peak was achieved at 9 Hz, which was assumed as the mechanical interaction of rock and the two cutter PDC bit at a constant motor speed. Optimum frequencies are close to multiples of 9 Hz, so it was also assumed that maximum ROP increase occurs at some resonance of excited and natural vibrations.

From the previous investigations it can be concluded that vibration-assisted rotary drilling seems to be a very promising and efficient drilling method, which can be used in the field soon. However, in order to apply vibrations on top of the bit, an efficient downhole vibration tool that can operate during deep drilling conditions is required. The next chapter will provide information on currently developed downhole vibration tools.

1.4 Significance of the Research

The VARD project investigation showed positive results, as was described in the previous section, however, these experiments were conducted on a small scale. The experiments were performed with an initial experimental setup and a small power vibration source. In order to move the research project forward, a drilling investigation should be performed on a bigger scale and in conditions that are closer to field ones. Moreover, at the last stage of the VARD project, experiments should take place while drilling in real field conditions.

The vibration table that was used for the Li [6] and Babatunde [8] experiments cannot satisfy project requirements for bigger scale due to its limited power and overall geometry. The next stage of vibration experiments requires a vibration source of higher power that could be easily installed in laboratory and in field conditions. This fact makes it necessary to develop an efficient vibrating prototype that can be used for further drilling investigation within the VARD project. Moreover, the required prototype should be able to fit both laboratory and field capabilities. This will provide more flexibility in terms of experimental work, as well as the ability to compare laboratory and field results. In addition, the tool should fit larger scale experiments, and consider drilling with a bit diameter of up to 6 inches.

Consequently, it can be concluded that further VARD project investigation, related to larger scale experiments, cannot proceed and be successfully performed without an efficient prototype vibration tool. In addition, this tool should be developed and tested

quickly, while ongoing investigation is performed, so that when larger experiments take place a prototype tool can be delivered and optimized for the required specifications.

2 Literature Review

2.1 Existing Down-Hole Drilling Tools

Several companies and research teams have made an attempt to develop a down-hole vibration, percussion or pressure pulsating tool which can improve ROP at significant depth drilling conditions. In the current review, hydraulically powered tools will be considered, as these eliminate the requirement for a down-hole electrical power supply. All discussed tools are powered by drilling mud, which is pumped into the drill string. These tools are designed to operate at high bottom-hole pressure, where ROP decreases significantly. Currently, several approaches have been made in terms of tool design and operation: mud hammers, pulsation tools, agitators and cavitation tools. In addition, other down-hole vibration tools, which were not initially designed for ROP improvement, will be considered in this review as they may be modified in order to improve drilling.

2.1.1 Novatek Mud Hammer

One of the most current mud hammer designs was proposed by Novatek Company (Figure 2.1). The summary of the tool testing was presented in the Novatek annual report [9]. Mud hammers are mainly used for percussive drilling, which is mostly applicable for hard rocks. Strong vertical impacts, produced by the hammer and transferred to the bit, create a tensile fracture of the rock.

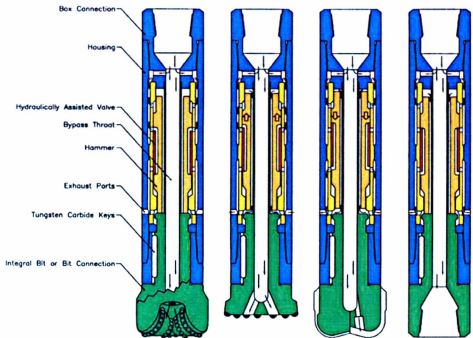


Figure 2.1 – Novatek mud hammer [9]

The tool converts a portion of drilling mud energy into mechanical impact on top of the bit, which causes an instantaneous weight on bit increase. Impact is caused by the hammer strike, which is pushed by the drilling mud as internal valves change the direction of the drilling mud flow across the hammer mechanism of the tool. Novatek’s final report [9] describes the action of the tool and states that the impact drives the bit into the formation. However, this description does not specify required compliance in the system, which is required to produce impact amplitude, which might be a significant factor.

This tool was tested at Terratek facilities with several types of sandstone and shale rocks; ROP improvement was reported in the range of 12 to 75%. The test was performed in the pressure range of 300 to 3000 psi. The 12% ROP increase was obtained at 2000 m of simulated depth and a 53% increase at 200 m of operating depth. However, the author states that overall maximum improvement of penetration rate with regards to conventional drilling might reach up to 75%; this maximum improvement refers to shallow depth. In addition to its performance, the new Novatek mud hammer does not use any springs and seals. This increases the life of the tool compared to previous versions. [9]

Nevertheless, mud hammers are not the best option for ROP improvement at great depth drilling. The first reason is the complicated design. Even though it does not include springs, the valve edges and impact area have significant wear. This results in early valve damage, and the overall life of the tool, specified by the manufacturer, is 720 hours. Another factor is the significant decrease in efficiency at high bottom-hole pressure. The reason is that the hammer impact takes place in the mud bath. This means that before impact the hammer must squeeze the liquid out. As a result, at high bottom-hole pressures the hammer impact reduces and the full impact cycle may not occur [9]. The Novatek mud hammer has some other disadvantages: it is not applicable for small diameter bits, and it has significant flow losses, because of the exhaust ports.

Technical specifications of the Novatek mud hammer are presented in Appendix A.

2.1.2 Tempress Tool

This tool has been developed by the Tempress Company and is presented in Figure 2.2. The tool performance was described in HydroPull Drilling reports by Tempress [10, 11]. The pulsation tool produces two types of impact:

- Pressure pulsations, which cause bottom-hole pressure fluctuations; and
- Vertical impact on the bit.

The Tempress tool does not create high axial force impact on the tool; its major effect corresponds to bottom hole pressure fluctuation. Therefore a proposed successful application of the Tempress tool is for pressure sensitive rocks such as Mancos shale.

According to Kollé [10,11], the Tempress tool should be installed on top of the bit and a coupling connection to the drill string should be used. This connection should have significant compliance to create positive displacement of the vibration oscillation. Coupling specifications will define magnitude of vibration amplitude, which is a significant parameter.

This tool has been tested in full scale simulation at the Terratek facilities, as well as in realistic field conditions. ROP improvement was recorded in a range from 33% (porous sandstone) to 200% (shale), however, this improvement was mostly caused by a higher stall WOB that can be applied with use of the tool. Some of the strong aspects of the Tempress tool are commercial availability and both pressure pulses and vibration force application on the bottom-hole [10, 11]. The commercially available product name has been changed to HydroPull, although the technology remains the same.

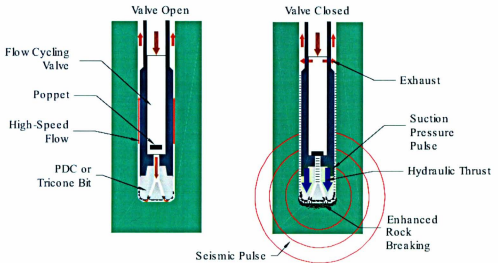


Figure 2.2 – Hydraulic pulse drilling tool [10]

Currently, the commercially available product HydroPull has a low frequency band in the range of 8 - 17 Hz. This may cause interference within pressure pulses of the tool and downhole telemetry system pulses. Also, HydroPull has exhaust ports and valves; this may have a negative effect on the robustness of the tool, especially when operating with abrasive drilling fluids. In addition, less efficiency was recorded, when operated with a higher WOB. The Tempress tool showed the best results only at high amplitude pressure pulses, which can be achieved at high flow rates.

Technical specifications of the HydroPull are presented in Appendix A.

2.1.3 Hydraulic Pulsed Cavitating Tool

This technology was proposed by China University of Petroleum, Beijing. Basically, the down-hole tool has both a pulse and cavitating jet (Figure 2.3). The tool was presented and described in papers published by Li et al. [12, 13]. This tool improves ROP by means of cavitation erosion, local negative pressure effect and by enhancing bottom hole cleaning due to jet pulsations [13].

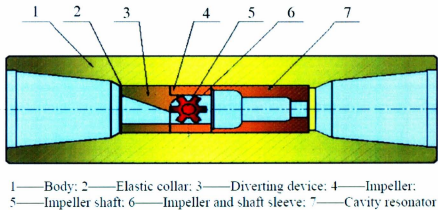


Figure 2.3 - Hydraulic pulsed cavitating jet generator [13]

According to the authors, the generator should be installed directly behind the bit. It produces three kinds of effects [12, 13]:

- Hydraulic pulse – enhancement of cutting cleaning;
- Cavitating erosion – improvement of rock-breaking; and
- Instantaneous negative pressure – producing instantaneous negative pressure pulse at the bottom hole, which causes local underbalanced conditions; when the

hydraulic pulsed jet is shaped around the nozzle, a low-pressure area will occur around the bit [13].

Specifications for the hydraulic pulsed cavitating jet are presented in Appendix A.

This down-hole cavitating tool has several advantages. First of all, it was tested in the field with the drilling depth range of 1300 to 6100 m. A field test was performed for underbalanced drilling at several Chinese oilfields. The reported ROP improvement was in the range of 10 to 100%. For instance, the best improvement was achieved at a depth interval of 2580 to 3349 m, and the ROP increased from 4.65 to 12.12 m/hour. Other advantages were an appropriate flow rate range, according to the authors, and a small pressure drop along the tool. The tool was designed to operate with an 8.5 inch diameter bit, and it requires a flow rate in the range of 400 to 500 gpm with a reported pressure loss under 1 MPa [13].

Despite these advantages, the tool has significant drawbacks. The first is a low frequency range of hydraulic pulses, which is about 10 Hz. This will cause interference with drilling telemetry system, as a mud pulse telemetry system is most widely used nowadays and it operates in the range of frequencies from 5 to 40 Hz. Another disadvantage is that mechanical components are exposed to drilling mud, which limits the tool life to 280 hours.

2.1.4 Agitator Tool

The Agitator tool was developed by Andergauge and National Oilwell Varco. Its major purpose is to reduce low side friction of the drill string by means of axial vibration

oscillation. The tool is presented in Figure 2.4. Performance data for the tool compatible with a 6 inch bit is presented in Appendix A. The developers state that the agitator provides bottom hole assembly excitement to improve weight transfer to the bit, which causes an increase in the ROP [14].



Figure 2.4 – Agitator tool [14]

The tool during operation produces two types of effects:

- Drilling mud pressure pulsations; and
- Vibration oscillations.

The Agitator tool is driven by a positive displacement power section (similar to a mud motor) that has a special assembly at the end of the stator, which slides on the surface with a flow passage. Sliding side to side, the end of the motor shaft restricts and opens the flow passage, creating pressure pulsations. Frequency of the pulsations in this case depends on the mud motor speed. Created pressure pulsations also oscillate vibrations on the body of the tool.

One of the major components of the Agitator tool is the compliance section, which is similar to a shock sub. The section consists of a series of compliance elements, designed as separate discs. This part of the tool provides amplitude to the vibration oscillations and can be managed by modifying the number of discs, which results in axial stiffness change.

The vibrations are reported to reduce friction of the drill string, improve weight transfer to the bit, reduce stick-slip, increase limits of extend reach drilling and increase drilling efficiency [14]. This tool has other significant advantages: it is commercially available, and performance was proven over a few years of field operation. It is fully compatible with MWD/LWD tools, and can be used with different bit types etc.

One disadvantage of the Agitator tool is a significant pressure drop, in the range of 450 to 700 psi. In addition, it has a number of mechanical components that are rotating and sliding, which may lead to a short lifetime of the tool.

2.1.5 Hydraulic Jar

A very common hydraulic down-hole vibrator that has been used for a long period of time in the drilling industry is the hydraulic jar. The main application of the jar is to free pipe, packers and other tools that may be lodged in the well. The jar is located in the tubing and it is a restrained slip joint. This joint can be released by applying tension force to the part that is connected to the upper pipe and hook. Then, the joint is released and accelerates till its body hits the anvil of the housing. Tension force accumulates due to valve and housing that meter the fluid flow [15]. The schematic diagram is presented in Figure 2.5. This technology is quite old, however, even more recent designs use the same concept, as indicated by recent patents [e.g. 16].

This concept, however, is not applicable to improve ROP, as this tool provides a single impact that follows tension stretching of the jar.

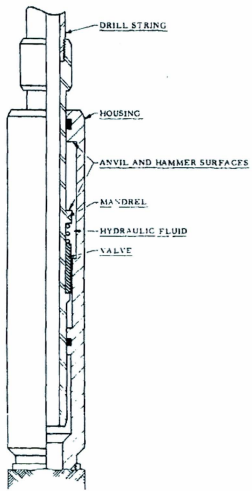


Figure 2.5 – Typical jar schematic diagram [15]

2.1.6 High Frequency Cavitation Hydrovibrator

The cavitation hydrovibrator was developed by the Institute of Technical Mechanics in Ukraine [17]. It was designed to enhance the efficiency of rotary drilling. This tool is presented in Figure 2.6. The characteristics and performance were described in a number of papers [17, 18, 19]. The tool is claimed to be applicable for soft, medium and hard formations.

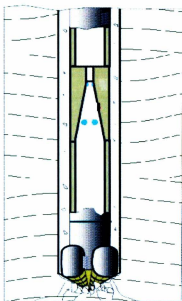


Figure 2.6 - High-frequency cavitation hydro-vibrator [18]

The tool during operation produces two types of effects:

- High-frequency and high-amplitude vibrations on the bit; and
- Drilling mud flow pressure pulsations.

Specifications of the high-frequency cavitation hydro-vibrator are presented in Appendix A [19].

The main advantage of this tool is its very simple design. It has no moving or rotating parts, or springs. Basically, the design includes an orifice of a small diameter and a diffuser. This assembly enables cavitations to be created and jammed, which cause pressure pulses and vibrations of the tool. It also has small dimensions and can be applied with a bit size down to 1.4 inches in diameter. In addition, pressure pulsations do not take place at the inlet of the tool, so the pumping system operates in the usual modes. The operational lifetime of the tool's 2000 hours, which is significantly higher than other competitive tools. This tool can be used for both full face and core drilling.

A possible disadvantage of the hydrovibrator is the very high pressure drop along the tool. However, high-frequency pressure pulses are 2 to 3 times higher than inlet pressure [19]. This tool will be described in more detail in Chapter 3, as this design and concept was chosen as a potential candidate for a VARD prototype.

2.2 Cavitation Theory

Cavitation is the process of transient vapour filled cavity creation in fluid at ambient fluid pressure, which exceeds the vapour pressure in the cavity, at a given temperature [20]. This process can be differentiated as passive and active. Passive cavitation occurs when fluid passes an obstruction or surface of an oscillating body. Cavities themselves are created in low-pressure areas. Active cavitation is the method of bubble creation with

the use of liquid hammer enhancement, which enables cavity formation at much higher ambient pressures.

A similar definition was provided by Angona [21]: “Cavitation is the phenomenon associated with the formation and violent collapse of bubbles in a fluid”. The author states that bubble collapse can cause erosion of materials with high strength.

Today, cavitation erosion is well known by marine and hydraulic engineers as a negative process, as it can significantly damage pump impellers, ship propellers, valves and other equipment. For example, centrifuge pumps with high flow rate capacity always have a minimum pre-charge pressure curve as one of the main pump performance characteristics. Operation with lower pre-charged pressures causes cavitation in the pump, which can result in significant damage.

Damage results from the high force which can be generated during cavity collapse. Jones and Edwards conducted “an experimental study of the forces generated by the collapse of transient cavities in water” [22] in 1960. Their idea was to produce a single transient cavity and collapse it on the end of a piezoelectric pressure-bar gauge, which is able to measure axial force variation on the bar.

Cavities were created by discharging a condenser with a high voltage through the gap between a tungsten needle and the end of the bar. The generated spark causes an extreme temperature rise in the fluid above the bar, which causes water to vaporize in that region. This method of cavity generation also provides the ability to vary its size by changing the spark gap width, charge and capacity of the condenser. A pressure-bar gauge was used to measure stress waves that propagate through the bar during cavity growth and collapse. This gauge uses a quartz disk to measure average stress over the cross-sectional area of

the bar. Experimental study was conducted over two pressure bars with diameters of $\frac{1}{2}$ and $\frac{3}{4}$ inches. A schematic assembly of the experimental setup is presented in Figure 2.7.

In their experiments, Jones and Edwards [22] used tap water that was held in the tank for at least 24 hours, in order to set the gas content equilibrium, which enabled them to assume that water is saturated with air at room temperature.

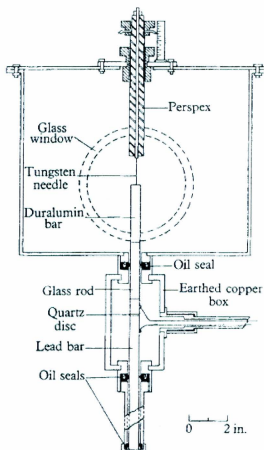


Figure 2.7 – Diagram of the experimental assembly [22]

During their experiments, the maximum peak force obtained was 105.9×10^6 dynes, which corresponds to 1.06 kN. Figure 2.8 presents the relation between cavity lifetime and peak force. This figure provides two sets of data: obtained for 0.5 inch bar (blank circles), and obtained for 0.25 inch bar (shaded circles).

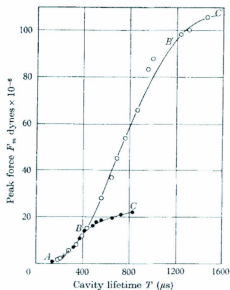


Figure 2.8 – Peak force of the cavity collapse versus its lifetime. Data presented for ½ inch bar (blank circles) and ¼ inch bar (shaded circles) [22]

In addition to force measurements, experiments involved a streak schlieren photograph, which is a flash photograph that records the invisible streak produced in a transparent medium as a result of variations in the density of the medium, leading to variations in the refractive index [23]. These photographs recorded the cavity collapse on the plane surface of a 0.5 inch diameter bar (Figure 2.9) and a sequence of spark shadow photographs of the cavity growth and collapse (Figure 2.10). Another significant

observation was made during these experiments. After the transient cavity has collapsed, another cycle of growth and collapse may occur, which is called the “rebound” phenomenon. According to the authors, this observation was also made by other investigators in cavitation experiments.

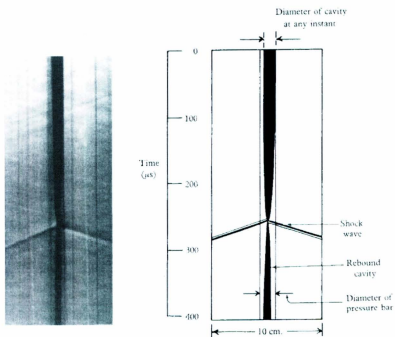


Figure 2.9 – Collapse and rebound of a cavity of lifetime 800 μ s obtained by streak schlieren photograph [22]

In order to estimate maximum pressures of the cavity collapse pulse, the authors used approximate minimum cavity diameter value, as this parameter is hard to measure. Based on their assumption, the peak stress at the end of the bar during collapse of a cavity lifetime of 800 μ s was 10^4 atm, which corresponds to 1013 MPa. However, the authors

state an assumption regarding maximum value of peak pressure at the seat of collapse:
“Consideration of the uncertainties in this estimate, however, together with values
proposed by other investigators, indicate that the pressures are probably higher than this
value and more likely to be $\sim 10^5$ atm” [22].

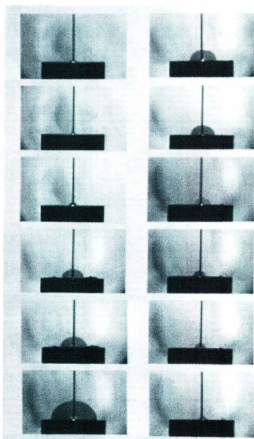


Figure 2.10 –Growth and collapse of a cavity with lifetime of 800 μ s obtained by streak schlieren
photograph [22]

Similar numbers are presented in a more recent paper by Guo et al. [24]. Their study was conducted in the field of oil recovery enhancement by means of high frequency vibration technology. This technology is based on ultrasonic energy. According to the authors, one of the most outstanding effects of this energy is cavitation. They stated that cavity collapse generates high pressure, as a significant amount of energy is concentrated at a very small spot, of which the maximum size is in the range of a centimeter. The authors presented data that yielded a maximum pressure pulse peak generated by single cavity collapse in the range of 10,000 to 100,000 atmospheres (10^5 atmospheres).

These experimental studies prove that the forces that are generated by cavity collapses are very high. Pressures that might be developed can overcome yield stress of many materials, including steel. That is why cavitation can damage ship propellers and pump impellers.

Although the energy of cavity collapse is harmful for some hydraulic machines and parts, it also can be beneficial for some other applications. As a result of scientific and engineering progress, some modern tools and techniques use cavitation energy for different purposes. The petroleum industry has found ways to apply this phenomenon to its benefit as well.

Bakker and Ivannikov [20] described the application of the cavitation in well engineering. They clearly specify the positive effects on well cleaning and fracturing while using cavitation tools. In this case, cavitation has two significant effects (Figure 2.11):

- 1) suction in the decomposing cavitation flare; and
- 2) shock waves which are generated by cavity collapse.

The conditions inside the cavitation flare are different from the outside, as the cavity pressure drops to the vapour pressure of the fluid. This creates effective local suction close to the flare.

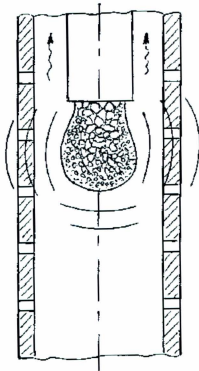


Figure 2.11 – Illustration of cavitation flare [20]

The second effect, shock wave, occurs when cavities are imploded. Unlike the suction effect, shock waves propagate much farther from the area of collapse. Because of

these effects, cavitation tools may be used for plugged screens and bore hole cleaning of debris [20, 25], as well as for rock fracturing.

According to the authors, rock fracturing by cavitation is completely different from conventional pump-in hydraulic fracturing. Shock waves created by cavity collapses have much greater magnitude, and are repeated with high frequency. Another difference is the orientation of the fractures. Unlike the pump-in single fracture, which is oriented perpendicular to the least principal stress, cavitation shock waves create multiple fractures in different directions around the wellbore.

The authors concluded in [20] that cavitation is a very powerful technology, which can be applied for various tasks of well engineering. From the field tests that were conducted, it was observed that effective cavitation can be produced at depths of up to 3000 m and even more. In addition, Bakker and Ivannikov mentioned drilling applications of the similar cavitation tool: "During field trials in Russia it was demonstrated that drill rates can be increased by up to 40% and bit life can be extended by up to 25% compared to the performance of previously applied bits" [20].

Another study that was conducted in the area of production enhancement was done by Bakulin [26]. He was investigating the influence of acoustic stimulation on fluid dynamics in porous media. Acoustic stimulation of porous media, according to [27], causes two effects: viscosity change of free oil, and cavitation in the radial space between the acoustic source and casing. According to the author, cavitation in porous media may occur in certain conditions. It is also stated in this study that small bubbles are created in the tension zones and then collapsed in the following compression area. This results in significant energy release and a local rise in the pore pressure. The energy amount, which

corresponds to pore pressure rise, is capable of inducing fluid migration in tiny pores, fractures and faults. The cavitation process was investigated in the laboratory and statistical data were obtained, as presented in Figures 2.12 and 2.13. From these figures, we can conclude that a higher frequency range is required to maintain cavitation at higher pressures.

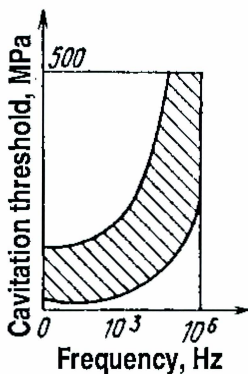


Figure 2.12 – Cavitation threshold as a function of frequency [26]

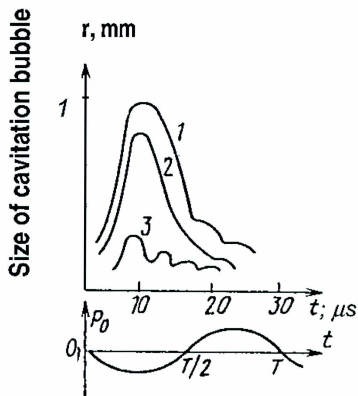


Figure 2.13 – Behaviour of a cavity as a function of its radius at constant frequency of 10 kHz and pressures of 10^5 Pa (line 1), $5 \cdot 10^5$ Pa (line 2) and 10^6 Pa (line 3) [26]

Cavitation was also investigated by Angona in 1974 [21] in an experimental investigation of a drilling mechanism that used cavitation erosion. The author conducted his tests at different hydrostatic pressures and came to the conclusion that cavitation intensity increases with an increase of hydrostatic pressure. In addition, he observed that for each constant acoustic pressure there is a range of hydrostatic pressure that causes cavitation with maximum erosion rate. Finally, Angona concluded that cavitation is an

effective mechanism for drilling and its effectiveness should increase with the hydrostatic pressure (depth) gain as long as the appropriate acoustic pressure can be generated to create cavitation.

From this section of the literature review we can conclude that cavitation is a very powerful technique which can be applied in petroleum engineering. In addition, it seems that the cavitation process can even be intensified at high hydrostatic pressures, so this technology is applicable for deep drilling and may be used as the source for prototype downhole vibrations.

3 Cavitation Drilling Tool Concept Description

A similar study of the downhole vibration tool, which uses cavitation as a means of vibration source, was conducted by a research team at the Institute of Technical Mechanics of the National Academy of Sciences of Ukraine. The purpose of their tool was to increase drilling efficiency at great depth. The first prototype and its performance were described in Manko et al. [17]. Their investigation was followed by early studies conducted in Russia by Kardysh et al. [28]. Russian scientists have concluded through research and drilling practice that axial vibrations of the required power, which are applied to the bit, have a positive effect on drilling intensification, bit wear and energy consumption. In addition, Tomsk University in Russia conducted research in this area and concluded that the mechanical speed of penetration can be increased by 2-3 times in the case of vibration-rotary drilling [29].

The goal for the research team from the Institute of Technical Mechanics (ITM) was to create a tool which would avoid the drawbacks of the vibrators: operation complexity, poor reliability due to moving parts and springs, low frequency range and other drawbacks [17, 18, 19]. As a result, they proposed a tool that does not have any moving parts, applies axial vibrations to the bit, and uses the power of the drilling fluid. This tool has a sleek design with the purpose of being a part of a drill string and it can be installed on top of the bit, or at some distance (e.g. above a core barrel).

Pilipenko and Manko [30] started with an investigation of pressure oscillation of the Venturi tube. As the next step of the investigation, they conducted experiments to

determine the best geometry of the Venturi tube, in order to obtain higher pressure pulses downstream of the tube. The results of this experimental work were published in 1977 by Manko [30]. He concluded that extremely high pressures were observed at the diffuser angle, ranging from 15° to 45°. In addition, the appropriate ratio of the outlet to inlet pressure (p_2/p_1) should be maintained in the range of 0.02 to 0.7. According to Manko, a diffuser angle of the Venturi tube higher than 45° eliminates the effect of inlet pressure on the frequency and outlet pressure does not exceed inlet values. In a case when the angle is less than 15°, no oscillations were observed. However, over a large number of experiments, the authors concluded that the best performance can be achieved within the diffuser opening angle range of 20° to 30°.

In order to prove that pressure pulses downstream of the Venturi tube are due to detached cavity collapse, researches from ITM conducted an experiment where pressure oscillations were measured by pressure transducers and slow motion video records were made to compare results (Table 3.1). As the results were quite similar, the authors concluded that pressure pulses in the flow are due to cavity collapse. In addition, researchers observed that cavitation parameter τ is approximately equal to the ratio of outlet to inlet pressure, therefore, cavitation parameter was calculated as the ratio for calculation simplification.

The process that occurs in the tool was described in the paper as well. The cavity grows in the diffuser part of the tool, detaches and then collapses at the centre of the flow producing a significantly high pressure pulse. The downstream wave propagates along a considerable distance, almost without damping, and the upstream wave is damped by an upcoming cavity. As the result, no pressure pulsations occur at the inlet of the tool, which

provides great benefit for the entire pumping system. In addition, the upstream wave helps to detach and form new cavities, so a self-oscillating process occurs [17].

Table 3.1 – Pulsation frequency at diffuser angle 15° and inlet pressure 725 psig [17]

τ	Pressure oscillation frequency determined from oscillograms, Hz	Frequency of detachment of the diffuser part of the cavity determined from video records, Hz
0.6	510	490
0.5	450	440
0.4	390	365
0.3	315	310
0.2	235	230
0.1	135	135

Another paper published by one of the researchers, Pilipenko, presented an analytical model that provides a throat diameter required to initiate cavitation [31]. This equation takes into account the mass, momentum and energy conservation laws. The orifice diameter can be calculated as

$$Fo = \frac{m}{\mu \sqrt{2\rho(p_1 - p_k)}} \quad (3.1)$$

where,

m = mass flow rate through the orifice (converging-diverging passage);

μ = flow coefficient of the passage;

ρ = density of the fluid;

p_1, p_k = pressures at the inlet and in the cavity, respectively.

The authors [17] also presented oriented operational conditions for field drilling, with regards to Equation 3.1 (Table 3.2). These data were used by Pilipenko for laboratory simulations of the tool.

The authors [17] also specified two more significant parameters with regards to the geometry of the tool. These are diameter and length of the outlet pipe, downstream of the cavitator (restrictor with orifice). They mentioned that these parameters had no influence on the frequency of pressure oscillation, however, they contribute significantly to the amplitude of pressure oscillations. Experimental studies showed that the diameter ratio of the outlet pipe and orifice should be equal to 4.1, and the ratio of the outlet pipe length to the orifice diameter should be equal to 100. Experimental results are presented in Figures 3.1 and 3.2.

Table 3.2 – Proposed operational conditions for hydrovibrator [17]

Parameter	Orifice diameter, mm			
	4		6	
Depth, m	100	1500	100	1500
Inlet pressure, psi	290	4350	290	4350
Flow rate, USgpm	5.3	40	13	63
Proposed wellbore	36	76	93	151

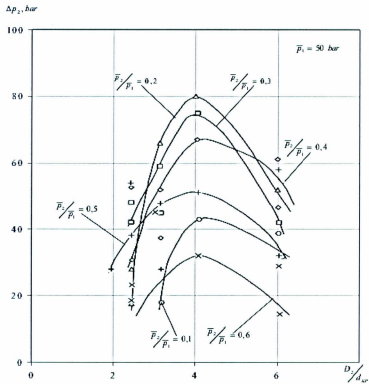


Figure 3.1 – Peak-to-peak amplitude of p_2 versus d_2/d_0 [17]

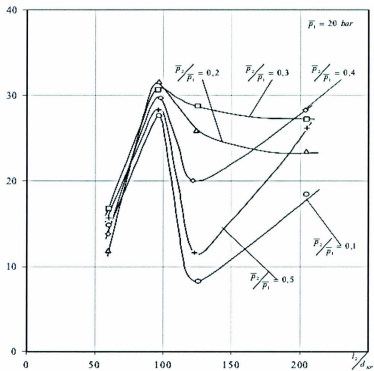


Figure 3.2 – Peak-to-peak amplitude of p_2 versus l_2/d_o [17]

Based on these geometrical recommendations, researchers from ITM have built the prototype model, which is presented in Figure 3.3. The orifice diameter was 4mm; outlet diameter and length of the outlet pipe were 17 mm and 400 mm, respectively.

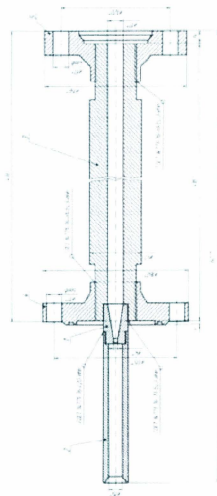


Figure 3.3 – Structural layout of the prototype hydrovibrator [17]

This tool was tested at the ITM laboratory facilities and its hydraulic system schematic was also provided in the paper (Figure 3.4).

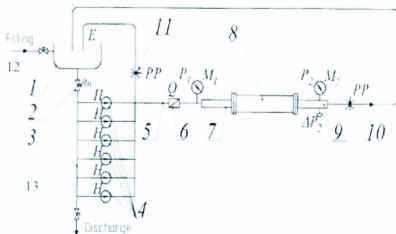


Figure 3.4 – Hydraulic facilities for the prototype testing at ITM [17]

The components of this system are described in Table 3.3.

Table 3.3 – Components of the ITM hydraulic system

# on the Figure	Component	# on the Figure	Component
1	Reservoir	8	Pre-prototype tool
2	Valves	9	Outlet pipe
3	Inlet header	10	Back pressure valve
4	High-pressure piston	11	Bypass throttle valve
5	Pressure pipeline	12	Industrial water filling
6	Flow meter	13	Industrial discharge valve
7	Inlet pipe		

This setup was used to test the performance of the hydrovibrator [17]. Figure 3.5 describes the behaviour of pressure oscillation of the outlet pressure p_2 . From the pattern of pulsations, the authors concluded that these oscillations are not harmonic and are due to cavity collapses in the tool. The oscillations shown were obtained at an inlet pressure of 2900 psi (201 bar) and a cavitation parameter of 0.15 [17]. As we can see from Figure 3.5, outlet pressure at its peak values exceeds the inlet pressure of 201 bars, although pressure drop across the tool is significant and drops as low as 20 bars.

The authors indicated that after the set of experiments were completed for the 4 mm orifice tool, they were able to provide operational boundary conditions. In order to create cavitation in the tool, the required flow rate should be in the range of 8 to 41 US gallons per minute (USgpm), with a corresponding inlet pressure range of 159 to 4365 psi [17, 18].

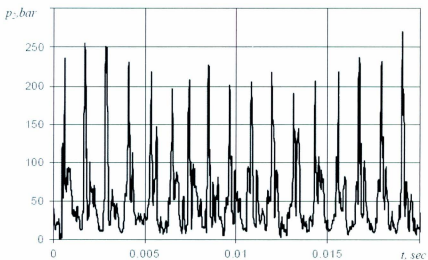


Figure 3.5 – Pressure oscillations at the outlet of the cavitator [17]

Figures 3.6 and 3.7 present the frequency and peak-to-peak amplitude of pressure pulsations as a function of cavitation parameter and inlet pressure.

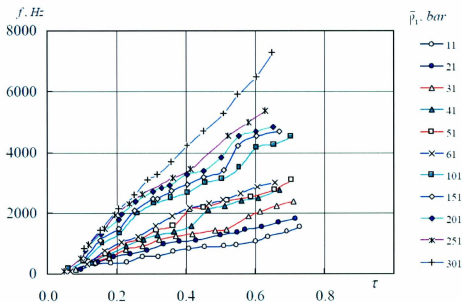


Figure 3.6 – Frequency of cavitation oscillations [17, 18]

From Figure 3.6 we can conclude that higher inlet pressure causes higher pulsation frequency and has a linear relation with the cavitation parameter, however, cavitation occurred in the range of τ values between 0.05 and 0.78 with the frequency range within 80 to 7300 Hz. From Figure 3.7 [17, 18] it can be concluded that maximum amplitude of pressure pulsations occurs in the range of τ parameter values of 0.10 to 0.36. Also, higher inlet pressure shifts the curve in the direction of cavitation parameter decrease. Consequently, we can say that in both cases inlet pressure increase results in performance

enhancement. In addition, cavitation parameter should be tuned to obtain higher frequency or higher amplitude.

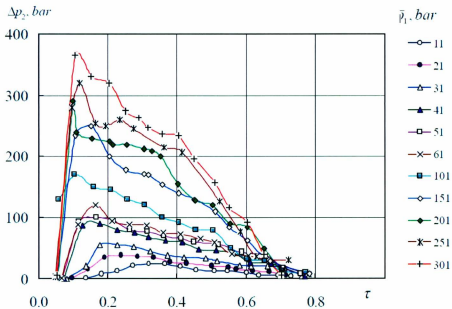


Figure 3.7- Peak-to-peak amplitude of cavitation oscillations [17, 18]

Another significant observation, which was done during the authors experimental investigation [17, 18], was their conclusion concerning vibration accelerations of the tool. They stated that pressure pulses that occur in the tool cause axial vibration accelerations of the tool itself. The acceleration magnitude can reach extremely high values, up to 10,000g. The experimental results are presented in Figure 3.8.

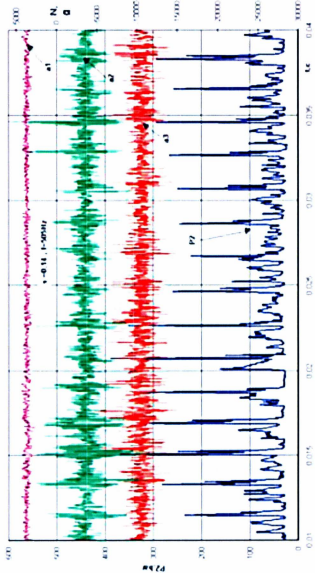


Figure 3.8 – Time oscillogram of the hydrovibrator vibration accelerations: a1 –upstream of the tool; a2 - on the hydrovibrator; a3 – downstream of the tool [17, 18]

In addition to the experimental data, Pilipenko and Manko, with other researchers, made an attempt to mathematically model axial vibrations of the hydrovibrator [17]. They created a system of differential equations, in order to simulate fluid oscillations at very high frequencies, with the use of 220 finite elements. This system enabled the authors to analyze different parameters at different sections of the prototype tool (Figure 3.9). As the outcome of this modeling, the ITM research team obtained qualitative and quantitative results, which agreed with experimental data.

The authors calculated results for: (a) time dependence of the displacement; (b) vibration accelerations; and (c) the volume of the cavity that collapses in the flow (Figure 3.10) [18].

As the result of experimental studies and the mathematical model, the authors recommended the specifications for the 4 mm hydrovibrator (Table 3.4) [18].

An additional experimental study by the ITM research team was published in 2006 [19]. Pilipenko compared tool performance with different orifice sizes: 4 mm, 6 mm and 8 mm, where the tools with bigger orifice diameters are for bigger diameter boreholes, as the flow rate gets considerably higher with an increase in diameter. The authors propose corresponding flow rates and borehole diameters for these three tools, with regards to an inlet pressure range of 160 to 4365 psi (Table 3.5) [19].

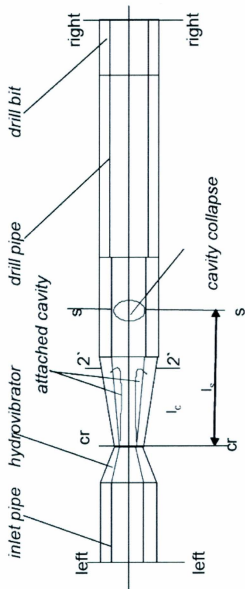
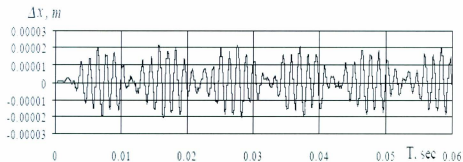
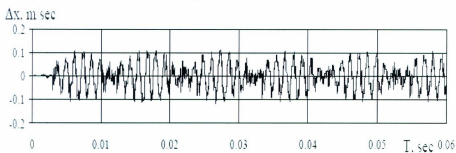


Figure 3.9 – Structural layout of the hydrovibrator prototype [18]



(a)



(b)

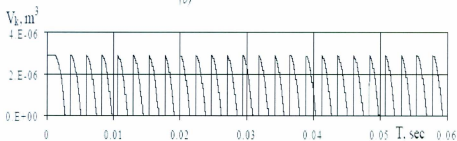


Figure 3.10 – Calculated time dependence of the tool parameters: (a) time dependence of the displacement, (b) vibration accelerations, (c) the volume of the cavity [18]

Table 3.4 – Hydrovibrator performance characteristics [18]

Parameter	Value	Parameter	Value
Borehole	36 to 250 mm	Max. mass	up to 40 kg
Max. drilling	4000 m	Tool max.	up to 1 m
Working fluid	water, clay or emulsion drilling mud	Mean tool lifetime	no less than 2000 hours

Table 3.5 – Operational parameters for hydrovibrators of different orifice size [19]

Orifice diameter, mm	Flow rate, gpm	Borehole diameter, mm
4	10 – 50	36 – 76
6	20 – 110	93 – 150
8	40 – 200	151 – 250

Pilipenko and others [19] presented their experimental data in the figures to compare performance of these tools (Figure 3.11). In addition to previous conclusions regarding inlet pressure and cavitation parameter, we can see that a smaller diameter orifice results in a higher frequency response of the hydrovibrator. On the other hand, a bigger restrictor diameter results in a higher peak-to-peak amplitude of pressure pulses, and as a result higher vibration acceleration on the tool.

Inspired by the results of ITM tool performance and its simplicity, the VARD team decided to build an experimental setup for cavitation tool performance confirmation and its usage as a possible prototype for further investigation of vibratory assisted drilling at high frequencies. So far, all drilling investigations within the VARD project were considered in a low frequency range. A tool similar to the ITM prototype [17, 18, 19] would enable investigations of high frequency and high force impact studies on vibration drilling at depth.

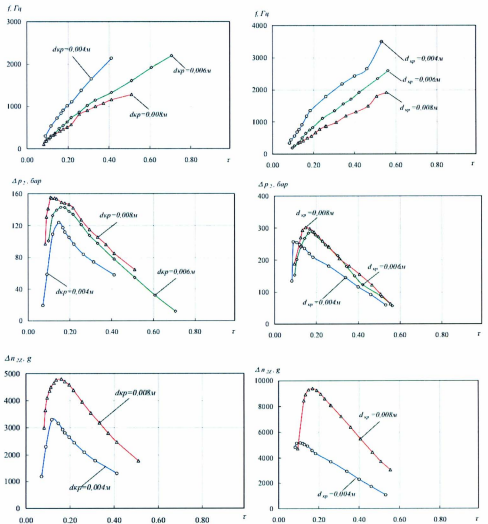


Figure 3.11 – Tools performance curves for inlet pressure 740 psi (left side), inlet pressure 1460 psi (right side) [19]

4 Prototype CFD Simulations

This chapter will describe CFD simulation results obtained using Flow 3D software. This software was chosen based on its capability to simulate cavitation.

The first step was to build a model that would be very similar to the desired prototype and to conduct a comprehensive study of the simulation results. The geometry for the model was based on Pilipenko's paper [17]. According to the experimental results from the paper, the diameter of the outlet pipe should be 4 times bigger than the orifice diameter, and its length – 100 times bigger (see more detailed description in Chapter 3). Orifice size was chosen at 4 mm, as this size was experimentally tested in the paper and some reference performance data were provided. Flow passage geometry parameters of the simulation model, except for those described above, were chosen based on preliminary design of the prototype tool (a full design description is provided in Chapter 5). A new and realistic simulation model was created and made ready for use with Flow 3D software (Figure 4.1). Inlet and outlet pressures of the tool were used as boundary conditions. Other input parameters did not work properly for simulations.

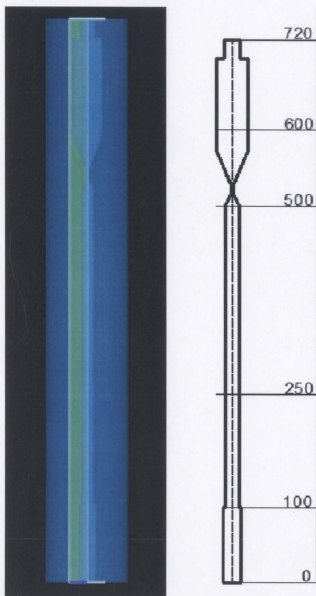


Figure 4.1 – CFD simulation model

4.1 Confirmation of Tool Operation within Experimental Capabilities

The first simulations were designed to investigate tool performance within the pressure ranges compatible with the laboratory pump system. Another purpose of the first stage simulations was to screen the factors using the Design of Experiments (DOE) technique. Design-Expert (DOE based software) was used to design and analyze the simulation results. DOE methods make it possible to show dependence of the factors, their interactions and significance with respect to the outcome results.

Table 4.1 describes the software input parameters, which were considered as constant. The mesh and tool geometry was not changed, throughout all simulations. During preliminary simulations it was observed that a few seconds run is enough for analysis, as run time significantly increases simulation time. However, data would be obtained from the time interval in the middle. It was observed that during the first second of simulation, software initiated processes and pressure pulsations do not occur. The reason for this is that Flow 3D starts from larger time steps which continuously reduces after the first second. During the last few seconds of simulation process, pressure pulsations were decreasing. This phenomenon is probably due to the specified pressure boundary condition, which software stabilizes by the end of a run. Taking into account these observations, it was decided to obtain data from 1s to 5s, which always showed appropriate results. Pressure data was obtained at the Z value of 150 mm (Figure 4.1) which was chosen since it is adownstream point that is at considerable distance from the nozzle but is not too close to the outlet with specified pressure. The fluid used in the simulation was water.

A two level fractional DOE design was used to screen the factors. In addition, a half-fraction was used; this gives the resolution IV design. This means that we are reducing the number of runs without sacrificing significant parameters. Resolution IV does not take into account three factor interactions, which are commonly believed to be ignorable. Table 4.2 presents input parameters that are going to be analyzed by the DOE software Design-Expert, according to which, 32 simulation runs were required for 5 input factors to fulfill the experiment design requirement.

Table 4.1 – Constant inlet parameters for simulations

Input parameter	Value
Overall simulation time, s	8
Simulated fluid	water at 20°C
Mesh and tool geometry	single block
Pressure measurement point, mm	Z=150
Data interval, s	1 - 5

Table 4.2 – First simulations variable input parameters

Parameter	Low	High
Inlet pressure, psi	300	850
Outlet pressure, psi	50	250
Cavitation pressure, Pa	2,300	900,000
Cavitation initiation time, s	0.0001	0.01
Gravity	no	yes
Viscosity	no	yes

A two level factorial design requires a parameter at two levels: high and low. Maximum inlet pressure is based on pump capabilities. Outlet pressure associated with

back pressure and its maximum is considered in order to provide at least a 50 psi pressure drop. Low level cavitation pressure is 2300 Pa, which is vapour pressure, and its maximum value is obtained from the software manual screenshot. Cavitation initiation time (Flow 3D input parameter that represents the time of cavity initiation (creation)) was chosen as one order above and below the software manual screenshot value (0.001). Gravity and viscosity are qualitative factors in these simulations. This means that software will take into account gravity and fluid viscosity if it is “yes”, and will not otherwise.

Table 4.3 provides outcome parameters that were obtained as data from simulation interpretation. The dominant frequency of the pressure pulses, as well as maximum multiple frequencies, were obtained from Fast Fourier Transform (FFT) analysis. MatLab code is used to perform the FFT; amplitude versus frequency plot is generated as the result of each run of the code. This code considers the time interval, which is specified by user and number of points for FFT analysis (2^n). According to these points, the code resamples data at a constant sampling rate using interpolation of the data. The reason for this procedure is that Flow 3D continuously changes the time step, so the data could not be processed by FFT directly. Maximum and average pressure peaks are recorded as the ratio of the peak magnitude to the inlet pressure value and they are obtained from the plot, which is produced by Flow 3D. Cavity initiation process is a qualitative parameter, which is judged from the simulation animation and is subjective.

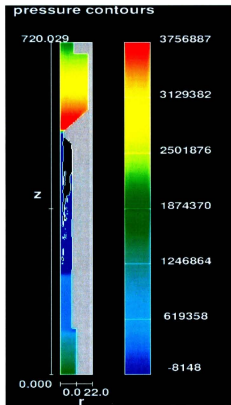
Table 4.3 – Output parameters of the first simulations

Parameter	Dimension	Explanation
Dominant frequency	Hz	From FFT
Maximum multiple	Hz	From FFT
Maximum pressure peak	Pa	Ratio P_{out}/P_{in} for maximum pressure peak
Average pressure peak	Pa	Ratio P_{out}/P_{in} for average pressure peaks
Cavity initiation process	1 to 3	1 – no cav. 2 – cont. growth 3 – periodically

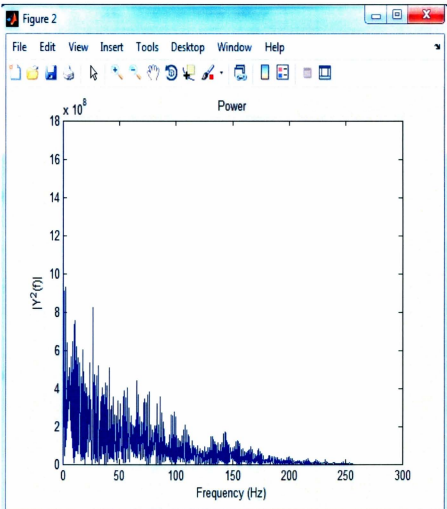
The results of the Design-Expert were summarized in Table 4.4. During these simulations cavitation occurred in 28 out of 32 runs. The only condition when cavitation did not occur was with a pressure drop of 50 psi, which is considered too small to initiate cavitation, according to [17]. However, some runs at 50 psi pressure drop still showed cavitation initiation. Furthermore, some created cavities collapsed and these collapses caused pressure pulsations. This was observed during animation of the process. However, not all cavities were collapsed as they moved downstream. Animations of the runs also showed that a big cavity was created and that it could extend far from nozzle without detaching from the diffusing part. It was also observed that dominant frequencies were very low: the highest one did not exceed 15 Hz. However, software shows that frequency is increasing with an increase in inlet pressure. Another significant observation was maximum pressure pulses, which at some points exceeded inlet pressure and reached up to 150% of the inlet value. Figure 4.2 presents screenshot samples of the simulation results. Black regions on the animation screenshot indicate cavities.

In Table 4.4, plus or minus signs indicate input parameter adjustment (low or high), which would increase output parameter. If in the same column two input parameters are

marked in the same colour, they are in interaction, which means that the factors are dependent on each other. For instance, in the column of dominant frequency, inlet pressure and cavitation time are marked with the same colour. This means that increase in inlet pressure and decrease in cavitation time lead to an increase in the dominant frequency.



a



b

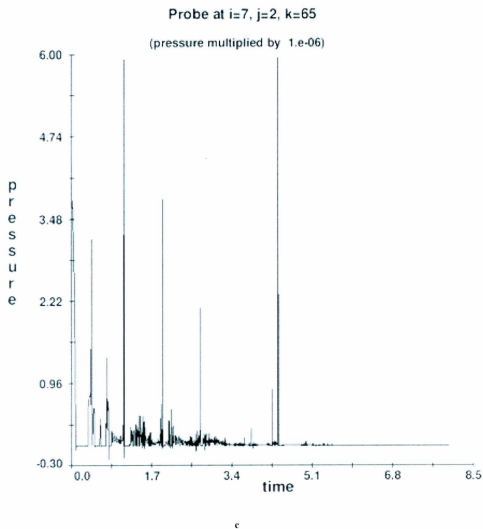


Figure 4.2 – Simulation results: (a) animation, (b) FFT plot, (c) pressure profile

Table 4.4 – First simulation results

Parameters	Dominant frequency	Max. Multiple frequency	Max. P peak	Avg. P peak	Cavitation process	
Inlet pressure	+	+	X	-	+	+
Outlet pressure	-	X	+	+	+	
Cavitation pressure	-	X	X	-	+	X
Cavitation time	-	X	X	X	X	
Gravity	X	X	X	-	+	+
Viscosity	+	+	+	X	-	

During interpretation of the results it was noticed that average pressure peak and cavitation process (qualitative parameter) are not significant outcome results, so it was decided not to obtain them in the next simulations. In addition, the gravity parameter was identified as not significant, but it was decided to leave it in the “on” option for later simulations. Unlike gravity, the viscosity option is significant, and as the results show, it should be in the option “on”. Another adjustment that could be done for the next simulations is cavitation initiation time, which was decreased, as this provides higher frequency response. Also, recommended cavitation pressure for use is 2300 Pa, as it makes more sense and shows better results. All these points are due to the experience gained from the current simulation, which will be accounted for in the next stage of simulations.

4.2 High Pressure Simulations

The next step, after confirmation of cavitation initiation, was to simulate tool performance at higher pressures. The first reason for this simulation is that the tool is intended to work at high pressures in the field. Secondly, it was observed that frequency of pressure pulses was increasing with increase of inlet pressure. Consequently, simulating at higher pressures and wider pressure range can confirm this observation or contradict it.

DOE methods were applied to the simulation, however, this time Response Surface Methodology (RSM) was used. In addition to two level factorial analysis, RSM takes into account center points and points beyond the investigating interval. This enables us to analyze factors more accurately and to observe non-linear behaviour of the parameters. Furthermore, 3D surface plots can be produced while using the RSM, which helps to visualize outcome results.

Constant factors are presented in Table 4.5. Simulation time, the timeframe of data recording, fluid, mesh, tool geometry and pressure measurement point are the same as for the previous simulation (see description in Section 4.1). Based on the conclusions made previously, it was decided to use a cavitation pressure of 2300 Pa. In addition, viscosity and gravity models should be included during simulations.

For high pressure simulations only three variable parameters were left to consider (Table 4.6). Inlet and outlet pressure are major factors that influence the outcome results. Maximum pressure corresponds to the hydrostatic pressure of water at approximately 2 km depth; the minimum output pressure value was chosen as 500 psi. Outlet maximum

and inlet minimum pressures were chosen to obtain a minimum of 500 psi pressure drop, as previously it was observed that at a small pressure drop cavitation may not occur. In addition to pressure factors, it was decided to investigate the cavitation initiation time parameter at smaller values, as this seems to increase pressure pulse frequency; its minor significance was observed during previous simulation runs. Consequently, the lower value from previous simulations (0.0001 s) was chosen as the “high” level for this parameter; the “low” level was chosen two orders lower (0.000001 s).

Table 4.5 – Constant inlet factors for high pressure simulations

Input parameter	Value
Overall simulation time, s	8
Simulated fluid	water at 20°C
Mesh and tool geometry	single block
Pressure measurement point, mm	Z=150
Data interval, s	1 - 5
Gravity and Viscosity models	On
Cavitation pressure, Pa	2300

As was mentioned in the previous section of this chapter, average outlet pressure and the cavitation initiation process were output parameters that were evaluated to be not useful. This time it was decided to avoid them. Multiple frequency outcome information was not very significant as well; nevertheless, it was decided to obtain this data. Finally, three output parameters were left to analyze high pressure simulation results (Table 4.7).

Table 4.6 – High pressure simulation variable input parameters

Parameter	Low	High
Inlet pressure, psi	1500	3000
Outlet pressure, psi	500	1000
Cavitation initiation time, s	0.000001	0.0001

Table 4.7 – Output parameters of high pressure simulations

Parameter	Dimension	Explanation
Dominant frequency	Hz	From FFT
Maximum multiple	Hz	From FFT
Maximum pressure peak	Pa	Ratio Pout/Pin for maximum pressure peak

Figure 4.3 presents input data for the Design-Expert software. As one can see, center points were used for this analysis (e.g. inlet pressure 2250 psi). These are used to analyze non-linearity of the outcome function. Overall 15 runs were required to conduct DOE analysis of the simulation results using RSM. During current simulations, cavitation has been observed for all 15 runs. Overall observation regarding cavity generation, its collapse and pressure pulse propagation is completely in agreement with previous simulation observations. This means that as the cavitation process initiates, some of the bubbles collapse and these collapses generate pressure pulses. In addition, some cavities were growing in size without detaching from the diffuser and some of the detached ones were not collapsed.

Current simulation results confirm previous observations regarding frequency dependence on input pressure. As we can see from Figure 4.3, the average frequency is 40

Hz, which is higher than the average of 15 Hz for previous simulations. This can be also concluded from Figure 4.4: the highest frequency is achieved at maximum inlet and minimum outlet pressure.

Select	Std	Run	Factor 1 A: Inlet pressure psi	Factor 2 B: Back pressure psi	Factor 3 C: Cavit time s	Response 1 Dominant F Hz	Response 2 Multiple F Hz	Response 3 Max P peak
	5	1	1500.00	500.00	0.00	32	125	2.5
	12	2	2250.00	1000.00	0.00	41	400	9.3
	11	3	2250.00	500.00	0.00	40	250	1.35
	10	4	3000.00	750.00	0.00	40	250	3.05
	14	5	2250.00	750.00	0.00	35	250	5.8
	15	6	2250.00	750.00	0.00	30	320	5.8
	1	7	1500.00	500.00	0.00	31	150	2.43
	9	8	1500.00	750.00	0.00	30	120	2.76
	4	9	3000.00	1000.00	0.00	40	300	3.48
	13	10	2250.00	750.00	0.00	32	320	5.8
	7	11	1500.00	1000.00	0.00	27	170	5.63
	2	12	3000.00	500.00	0.00	50	300	3.06
	3	13	1500.00	1000.00	0.00	27	200	5.8
	8	14	3000.00	1000.00	0.00	40	250	3.48
	6	15	3000.00	500.00	0.00	52	300	3.19

Figure 4.3 – Screenshot from DOE software data input

Maximum pressure peaks reached very high values, up to 21000 psi (run 2, Figure 4.3). The pressure fluctuation of this run is presented in Figure 4.5 (pressure values are in Pa). Another observation can be made about the maximum pressure peak: outlet pressure peaks were always higher than inlet pressure. Surface response of the maximum pressure peak is presented in Figure 4.6. As we can see, maximum pressure peaks can be obtained at maximum back pressure and an inlet pressure of 2250 psi.

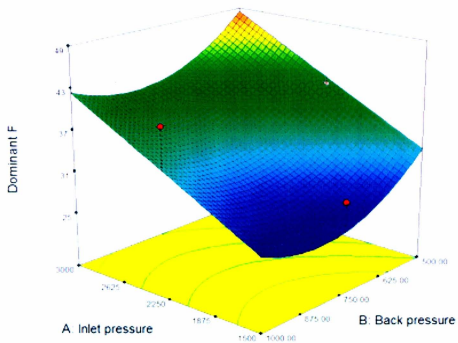


Figure 4.4 – Dominant frequency response surface

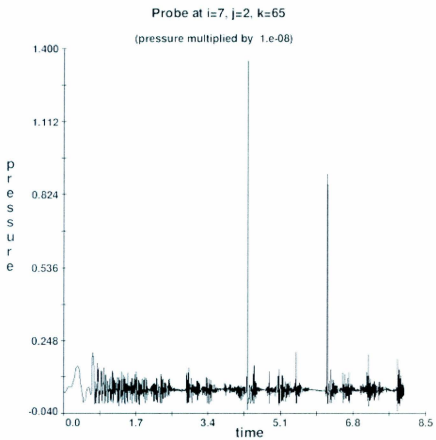


Figure 4.5 – Outlet pressure pulses

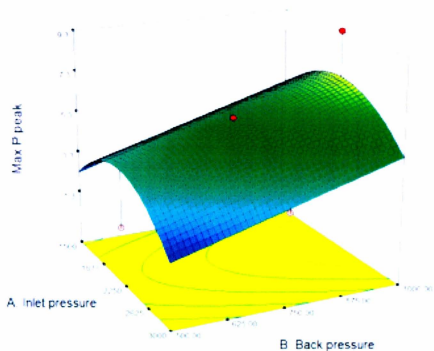


Figure 4.6 – Maximum pressure peak response surface

Multiple frequency response is presented in Figure 4.7. As we can see, inlet pressure is the only significant parameter that influences maximum multiple frequency.

During the current simulations, it was concluded that cavitation time was not significant.

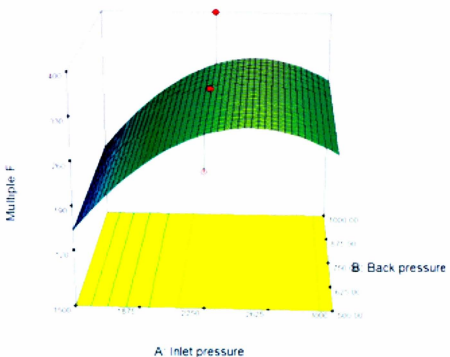


Figure 4.7 – Multiple frequency response surface

4.3 Estimation of Density and Viscosity Influence on Tool Performance

The previous two sections of the current chapter describe promising simulation results, however, these simulations were performed assuming water as a drilling fluid. In the field, engineering drilling fluids are commonly used for drilling operations. These fluids have higher density and viscosity than water. In addition, drilling mud is thixotropic: fluid becomes a gel under a static condition. This property of drilling mud prevents cuttings from falling down the borehole in case of a circulation stop.

Consequently, it was decided to investigate the influence of density and viscosity on tool performance. Furthermore, a test simulation run should be conducted with fluid properties that correspond to actual drilling mud with appropriate gel strength.

In this case, DOE analysis was applied as well. Previous simulations, described in section 4.2, were analyzed using RSM, and this technique was quite useful and provided good visualization. Therefore, it was decided to apply RSM to current simulations in order to conduct comprehensive analysis. Due to a number of factors, Design-Expert software required 25 simulation runs.

Considering the experience and conclusions from previous simulations, constant factors were chosen once again. Mesh and tool geometry, pressure measurement point, measurement timeframe, cavitation pressure, gravity and viscosity models were considered constant as in the previous simulations (Table 4.5). Overall simulation time was intentionally reduced from 8 to 6 seconds; data were obtained from second 1 to 5. It was observed that there is no necessity to run 3 seconds after the measurement has been done. In addition to this, cavitation initiation time was considered constant in this case, as previous simulations showed that at a small value it becomes insignificant. It was decided to fix this value at 0.000001 s.

Current simulations were performed with consideration of four variable factors (Table 4.8). It was decided to run these simulations in a high pressure range to avoid a small pressure drop, as it was mentioned previously that cavitation may not occur in such conditions. Density and viscosity ranges were obtained from a drilling fluid handbook and SPE textbook graphs [32, 33]. A low density level corresponds to water and a high level corresponds to high density drilling mud (normally, drilling mud density is 1100-

1300 kg/m³). Viscosity range was chosen from the graph in [32, 33], where 40 cP is a high value. As a result, we have a wide range of practically used mud properties, in terms of density and viscosity. Output parameters remain the same as for previous simulations (Table 4.7).

Table 4.8 – Variable factors for density and viscosity simulation investigation

Parameter	Low	High
Inlet pressure, psi	1500	3000
Outlet pressure, psi	500	1000
Density, kg/m ³	1000	1500
Viscosity, cP	10	40

Input factors and resulted outcomes were input in the DOE software (Figure 4.8). As we can see, runs 15 and 25 have no output data, due to software crashes, and they were ignored by the DOE analysis. During simulation performance, the same fluid behaviour as in the previous simulations was observed (see Sections 4.1 and 4.2). This means that cavitation may occur even at a high density and viscosity of the drilling fluid.

Select	Std	Run	Factor 1 A: Inlet pressure psi	Factor 2 B: Back pressure psi	Factor 3 C: Viscosity cP	Factor 4 D: Density kg/m ³	Response 1 Dominant F Hz	Response 2 Multiple F Hz	Response 3 Max P peak	
<input type="checkbox"/>	21	1	2250.00	750.00	10.00	1250.00	35	150	3.29	
<input type="checkbox"/>		5	1500.00	500.00	40.00	1000.00	35	175	1.74	
<input type="checkbox"/>		16	3000.00	1000.00	40.00	1500.00	32	180	2.9	
<input type="checkbox"/>		15	1500.00	1000.00	40.00	1500.00	27	150	5.8	
<input type="checkbox"/>		13	5	1500.00	500.00	40.00	1500.00	20	80	1.35
<input type="checkbox"/>		17	8	1500.00	750.00	25.00	1250.00	26	100	2.73
<input type="checkbox"/>		14	7	3000.00	500.00	40.00	1500.00	32	150	3.4
<input type="checkbox"/>		18	8	3000.00	750.00	25.00	1250.00	38	250	3.53
<input type="checkbox"/>		2	9	3000.00	500.00	10.00	1000.00	50	120	1.11
<input type="checkbox"/>		11	10	1500.00	1000.00	10.00	1500.00	20	150	6.77
<input type="checkbox"/>		1	11	1500.00	500.00	10.00	1000.00	32	125	2.75
<input type="checkbox"/>		6	12	3000.00	500.00	40.00	1000.00	38	300	4.06
<input type="checkbox"/>		4	13	3000.00	1000.00	10.00	1000.00	42	350	4.25
<input type="checkbox"/>		19	14	2250.00	500.00	25.00	1250.00	52	400	5.48
<input type="checkbox"/>		24	14	2250.00	750.00	25.00	1250.00			
<input type="checkbox"/>		10	16	3000.00	500.00	10.00	1500.00	34	100	0.9
<input type="checkbox"/>		22	17	2250.00	750.00	40.00	1250.00	40	175	3.22
<input type="checkbox"/>		8	18	3000.00	1000.00	40.00	1000.00	38	125	2.13
<input type="checkbox"/>		3	19	1500.00	1000.00	10.00	1000.00	25	150	3.29
<input type="checkbox"/>		20	20	2250.00	1000.00	25.00	1250.00	33	175	3.22
<input type="checkbox"/>		9	21	1500.00	500.00	10.00	1500.00	22	150	3.67
<input type="checkbox"/>		12	22	3000.00	1000.00	10.00	1500.00	35	125	3.43
<input type="checkbox"/>		23	23	2250.00	750.00	25.00	1000.00	36	150	1.46
<input type="checkbox"/>		7	24	1500.00	1000.00	40.00	1000.00	32	100	2.69
<input type="checkbox"/>		25	25	2250.00	750.00	25.00	1250.00			

Figure 4.8 – Screenshot from DOE input for density and viscosity investigation

The dominant frequency response plotted as 3D surface in Figure 4.9.

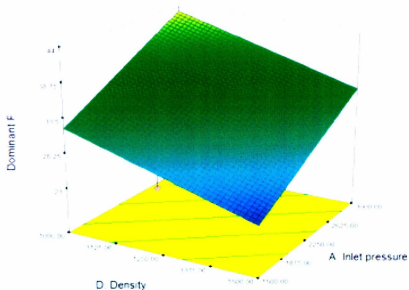


Figure 4.9 – Dominant frequency response

As we can see from Figure 4.9, maximum dominant frequency is sensitive to density and inlet pressure. Once again, it was observed that frequency increases with inlet pressure increase. Increase in density has a negative effect on the frequency. In addition, it seems that both parameters have a linear relationship. These simulation results show that viscosity does not have a significant influence on the frequency response of the tool.

Figure 4.10 presents the 3D surface for maximum outlet pressure peak values. In this case the software eliminates density, because it is not a significant factor for this response function, so only two significant parameters remain in the model: pressure and viscosity. From this plot we can conclude that the highest outlet pressure peak was achieved at minimum inlet pressure and minimum viscosity. Nevertheless, it seems that at higher viscosity high inlet pressure is more favourable in order to obtain higher pressure peaks.

However, it can be clearly concluded that an increase in viscosity reduced maximum pressure peaks at the outlet of the tool.

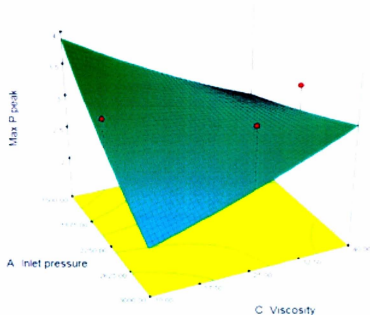


Figure 4.10 – Maximum pressure peak plot

DOE software did not fit an accurate model for multiple frequency response (possibly due to lack of considered points). As this factor is not significant, it was decided not to analyze it. Another observation is that in current simulations, the back pressure factor becomes insignificant when viscosity and density factors are applied.

The viscosity parameter was specified as constant for the discussed simulations. However, as was mentioned before, drilling mud has a thixotropic property. As a result, viscosity normally is specified in the stress versus shear rate plot, or could be specified

directly in viscosity versus shear rate (Figure 4.11). These viscosity (Pa*s) and density (kg/m³) data presented in [34] were specified in the software (Figure 4.12).

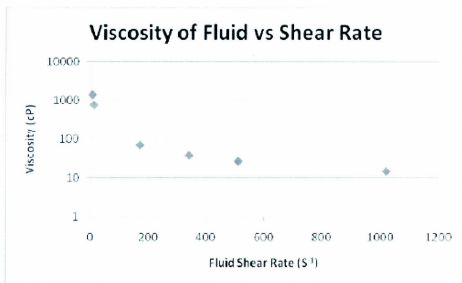


Figure 4.11 – Viscosity versus shear rate [34]

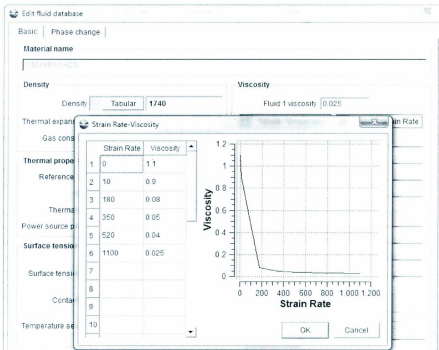


Figure 4.12 – Flow 3D fluid database screenshot

As the result of the simulation of the fluid with a thixotropic property, the same observation has been made as for the previous runs. The cavitation process and pressure pulsations were taking place during the simulation. This was observed from animation of the process and the pressure plot.

4.4 Simulation Conclusions

The first simulations described in Section 4.1 suggest high probability of cavitation process initiation in the prototype within the capability of the laboratory facilities. This

gave promise for experimental investigation of the tool. The results also confirm some statements that were made in Pilipenko's paper [17]:

- cavities are generated and their collapse produces significant pressure pulses;
- outlet pressure pulse amplitude can exceed inlet pressure;
- frequency increases with increase in inlet pressure;
- cavitation may not occur in the case of a small pressure drop.

However, simulations interpretation showed some disagreement with the information in [17]. First of all, frequencies are lower than experimental data obtained by Pilipenko. In addition, no continuous detachment and collapse of bubbles were observed. Some bubbles were not detaching; instead they were increasing in size. Not all detached cavities even collapsed, as some of them moved to the tool outlet.

High pressure simulations proved that the cavitation process initiates at a higher pressure drop. It was also confirmed that pressure pulse frequency increases with an inlet pressure increase. Pilipenko [17] states that maximum frequency is achieved at a higher pressure ratio ($p_2/p_1=0.8$) and maximum pressure peaks occur at a lower ratio ($p_2/p_1=0.15$). In the current simulation, Section 4.2, maximum frequency is achieved at minimum outlet pressure and a maximum inlet, which gives a lower value of the ratio. The same situation occurs with the maximum pressure peak: its maximum values are recorded at the highest outlet pressure and an average inlet, the pressure ratio in this case is higher than 0.15. In our case it seems that a higher frequency can be achieved at a smaller pressure ratio, and maximum pressure peaks can be obtained at a higher ratio. Also, pressure pulse frequency is very low compared to the frequency reported in the Pilipenko paper and pulse amplitude is much higher.

An investigation of density and the influence of viscosity on the performance of cavitation tool showed promising results as well. First of all, simulation results suggested that cavitation will occur at high density and viscosity using both constant viscosity and the thixotropic properties. It was also observed that frequency of the pressure pulses is sensitive to density increase, and maximum pressure peaks to viscosity.

Considering these conclusions, prototype development and manufacturing was considered feasible, as simulations suggested a cavitation process over different pressure ranges and with different fluid properties.

5 Prototype Development

This chapter will introduce the calculations and ideas that were implemented into the design of the prototype tool, as well as being a brief introduction to the overall experimental system.

5.1 Prototype Orifice Size Consideration

The Pulse-Cavitation prototype geometry was chosen to be the same as for the simulated model, as this geometry showed promising results during CFD simulations. As was mentioned in the previous chapter, the simulation model geometry was obtained from Pilipenko's paper [17].

Before producing a final design of the prototype, calculations were done to make sure that orifice size would be in agreement with the available flow rate. Orifice size is the major parameter of the tool geometry, as other dimensions are dependent on the nozzle diameter. These calculations were performed to make sure that the required pressure drop will be achieved within the flow rate of 5 to 40 USgpm, which is the current experimental capability within the Advanced Drilling Laboratory.

One of the Pilipenko papers described corresponding flow rates for different sizes of orifice nozzle [19]. The flow rates were calculated for other orifice diameters as well and results presented in Table 5.1. This table suggests three options for orifice diameter, which are 3, 4 and 5 mm. Other reference values, which are useful for these calculations

were given in paper [17]: the pressure drop across the 4 mm orifice at a flow rate of 5.3 gpm was 290 psi and at a flow rate of 40 gpm the pressure drop was 4350 psi.

Table 5.1 – Flow rate boundaries for different nozzle sizes

Diameter, mm	Qmin, gpm	Qmax, gpm
8	40	200
6	20	110
5	15	80
4	10	50
3	5	30
2	2	15

It was decided to have three approaches to estimate pressure drop across the nozzle and to compare them to referenced values.

The first approach was regular shock head loss calculations

$$h = K * \frac{v^2}{2 * g} \quad (5.1)$$

where

K = hydraulic coefficient,

V = velocity of the flow (speed in the orifice section was considered),

g = gravity constant.

However, calculations with Equation 5.1 are not very reliable, as the K value is not very certain. As the result, two K values were considered (Table 5.2). The first value of 0.2 was calculated from the gradual contraction equation and the second value of K=6 was calculated in reverse from reference pressure drops for 4 mm and 5.3 gpm [35].

Several conclusions can be made from this table:

- regular shock head loss calculation is not very appropriate, as K value varies with speed in the pipe;
- the calculations are not accurate as well: the referenced pressure drop for 40 gpm was 4350 psi, but calculations estimated a drop of 17561 psi.

Based on these calculations a 5 mm orifice seems to be too large in the case of coefficient $K=0.2$, which represents gradual contraction. Based on Pilipenko's suggestion [17], the pressure drop should be at least 300 psi in order to observe the fine cavitation process. As we can see, high pressure losses cannot be achieved and cavitation may not occur.

The second approach to calculate pressure drop across the orifice was using the nozzle Equation 5.2 [35]:

$$Q = 19.636 * C * d^2 * \sqrt{h} * \sqrt{\frac{1}{1 - \left(\frac{d1}{d2}\right)^4}} \quad (5.2)$$

where

Q = maximum flow rate, gpm

C = coefficient,

d1 = nozzle diameter, inches

d2 = inlet pipe diameter, inches

h = head loss, feet.

Calculations were performed for a flow rate range of 1 to 40 gpm, and the resulting calculated pressure drops are presented in Table 5.3.

Table 5.2 – Pressure loss across the orifice calculated by first method

Flow rate, gpm	Pressure loss across orifice, psi					
	K=0.2			K=6		
	3 mm	4 mm	5 mm	3 mm	4 mm	5 mm
1	1.2	0.4	0.1	34.7	11.0	4.5
2	4.6	1.5	0.6	138.8	43.9	18.0
3	10.4	3.3	1.3	312.2	98.8	40.5
4	18.5	5.9	2.4	555.0	175.6	71.9
5	28.9	9.1	3.7	867.2	274.4	112.4
6	41.6	13.2	5.4	1248.8	395.1	161.8
7	56.7	17.9	7.3	1699.7	537.8	220.3
8	74.0	23.4	9.6	2220.1	702.4	287.7
9	93.7	29.6	12.1	2809.8	889.0	364.1
10	115.6	36.6	15.0	3468.9	1097.6	449.6
11	139.9	44.3	18.1	4197.3	1328.1	544.0
12	166.5	52.7	21.6	4995.1	1580.5	647.4
13	195.4	61.8	25.3	5862.4	1854.9	759.8
14	226.6	71.7	29.4	6799.0	2151.2	881.1
15	260.2	82.3	33.7	7804.9	2469.5	1011.5
16	296.0	93.7	38.4	8880.3	2809.8	1150.9
17	334.2	105.7	43.3	10025.0	3172.0	1299.2
18	374.6	118.5	48.6	11239.1	3556.1	1456.6
19	417.4	132.1	54.1	12522.6	3962.2	1622.9
20	462.5	146.3	59.9	13875.4	4390.3	1798.3
21	509.9	161.3	66.1	15297.6	4840.3	1982.6
22	559.6	177.1	72.5	16789.3	5312.2	2175.9
23	611.7	193.5	79.3	18350.2	5806.1	2378.2
24	666.0	210.7	86.3	19980.6	6322.0	2589.5
25	722.7	228.7	93.7	21680.3	6859.8	2809.8
26	781.6	247.3	101.3	23449.5	7419.6	3039.0
27	842.9	266.7	109.2	25287.9	8001.3	3277.3
28	906.5	286.8	117.5	27195.8	8604.9	3524.6
29	972.4	307.7	126.0	29173.1	9230.5	3780.8
30	1040.7	329.3	134.9	31219.7	9878.1	4046.1
31	1111.2	351.6	144.0	33335.7	10547.6	4320.3
32	1184.0	374.6	153.5	35521.1	11239.1	4603.5
33	1259.2	398.4	163.2	37775.8	11952.5	4895.7
34	1336.7	422.9	173.2	40099.9	12687.9	5197.0
35	1416.4	448.2	183.6	42493.5	13445.2	5507.2
36	1498.5	474.1	194.2	44956.3	14224.5	5826.3
37	1583.0	500.9	205.2	47488.6	15025.7	6154.5
38	1669.7	528.3	216.4	50090.2	15848.9	6491.7
39	1758.7	556.5	227.9	52761.3	16694.0	6837.9
40	1850.1	585.4	239.8	55501.7	17561.1	7193.0

Several conclusions can be made from this calculation:

- nozzle flow calculations seem to be better than previous one, but still calculation results do not match reference numbers from the paper [17] for a 4 mm orifice;
- a 3 mm orifice seems to be too small, as a pressure drop of 995 psi is reached at 8 gpm, considering that the minimum flow rate for the pump is 5 gpm and maximum pressure is 1000 psi.

Table 5.3 – Pressure drop calculation by second method

Flow rate, gpm	Pressure loss across orifice, psi			Flow rate, gpm	Pressure loss across orifice, psi		
	3 mm	4 mm	5 mm		3 mm	4 mm	5 mm
1	15.5	4.9	2.0	21	6857.5	2167.5	887.7
2	62.2	19.7	8.1	22	7526.2	2378.9	974.3
3	139.9	44.2	18.1	23	8225.9	2600.1	1064.9
4	248.8	78.6	32.2	24	8956.8	2831.1	1159.5
5	388.7	122.9	50.3	25	9718.7	3071.9	1258.1
6	559.8	176.9	72.5	26	10511.	3322.6	1360.8
7	761.9	240.8	98.6	27	11335.	3583.1	1467.5
8	995.2	314.6	128.8	28	12191.	3853.4	1578.2
9	1259.	398.1	163.1	29	13077.	4133.6	1692.9
10	1555.	491.5	201.3	30	13995.	4423.6	1811.7
11	1881.	594.7	243.6	31	14943.	4723.4	1934.5
12	2239.	707.8	289.9	32	15923.	5033.0	2061.3
13	2627.	830.6	340.2	33	16933.	5352.5	2192.1
14	3047.	963.4	394.5	34	17975.	5681.8	2327.0
15	3498.	1105.	452.9	35	19048.	6021.0	2465.9
16	3980.	1258.	515.3	36	20152.	6369.9	2608.8
17	4493.	1420.	581.8	37	21287.	6728.7	2755.8
18	5038.	1592.	652.2	38	22454.	7097.3	2906.8
19	5613.	1774.	726.7	39	23651.	7475.8	3061.8
20	6220.	1966.	805.2	40	24880.	7864.1	3220.8

The last approach considers Equation 5.3 that was given in the Pilipenko paper [17]

$$Fkr = \frac{m}{\mu \cdot \sqrt{2 \cdot \rho \cdot (P1 - Pk)}} \quad (5.3)$$

where

Fkr = cross sectional area of the orifice, m²,

M = mass flow rate, kg/s,

μ = flow coefficient,

ρ = fluid density, kg/m³,

P1, Pk = pressures at the orifice inlet and in the cavity, Pa.

Maximum pressure of the pump is 1000 psi; however, in order to protect the pump, the maximum pressure is considered to be 900 psi (pressure of the relief valve). In addition, 50 psi was assumed for pressure losses downstream and upstream of the cavitation tool. Therefore, assumed maximum pressure loss across the tool is 800 psi (P1 - Pk=800 psi).

Calculations are presented in Table 5.4. The cross sectional area of the orifice was fixed according to the considered diameters and the flow coefficient was in the range of 0.5 to 1. As a result, we obtained the flow rate, which will create a 800 psi pressure drop across the tool.

Table 5.4 also eliminates usage of the 3 mm orifice, as the maximum flow rate is very low, considering that minimum flow rate of the pump is 5 gpm. This means that the choice of the orifice diameter size is between 4 and 5 mm. However, considering results from Table 5.2 (K=0.2) a 5 mm orifice might be too big and it will also increase the length of the tool, as its value is dependent on the nozzle diameter.

Table 5.4 - Flow rate that will produce 800 psi pressure drop across the orifice

Flow coefficient	Flow rate, gpm		
	3 mm	4 mm	5 mm
0.5	5.9	10.5	16.3
0.6	7.1	12.5	19.6
0.7	8.2	14.6	22.9
0.8	9.4	16.7	26.1
0.9	10.6	18.8	29.4
1	11.8	20.9	32.7

The final choice was made in favour of the 4 mm orifice, the same as in the simulated model, as this seems to satisfy the pumping system at any condition. Although the described calculations are not very consistent, they help to conclude that the chosen size of the cavitator is the best option for the proposed prototype of the cavitation tool. In addition, simulations were performed considering a 4 mm orifice.

The performed calculations along with simulation results, described in the previous chapter, gave a strong confidence in the design approach of geometry choice for the prototype.

5.2 Pulse-Cavitation Prototype Design

As the finalized prototype flow passage geometry has been confirmed, the tool drawings should be designed in order to proceed to the fabrication stage. It was decided to produce a prototype tool that could be used in a real field drilling scenario with a 6 inch diameter bit that would be compatible with different flow rates.

At the experimental stage the tool is going to be used with a 4 mm orifice, as from simulations and calculations presented in the previous section, this seems to be the best option, and will fit laboratory capabilities. However, if at some later stage the flow rate should be significantly increased, the prototype should have a bigger nozzle diameter. Consequently, the cavitation tool should provide an option of changing orifice size. As a result, it was decided to manufacture a nozzle as a separate part of the assembly (cavitating part), which can be easily replaced. The cavitating part dimensions were chosen in order to be able to manufacture a nozzle with a diameter from 3 to 8 mm, with different inlet and outlet angle configurations.

The prototype body was designed to consist of two parts, which would interlock the cavitating part in between (Figure 5.1). This assembly eliminates thread or any other type of connection between the cavitating part and other parts of the tool. This also provides easy access to the nozzle, which might be replaced. Regular o-ring is used to avoid leakages from the inlet to the outlet around the cavitating part.

As the cavitation tool should be compatible to use with a 6" bit, it should fit the appropriate drill collar size. The inlet and outer diameter of the tool should be the same as the collar to make the prototype a smooth part of the drill string. As a result, these values were fitted for a 4 1/4" drill collar, which is one of the options for a 6" bit. Selection of the drill collar and corresponding dimensions were chosen from the catalogue [36].

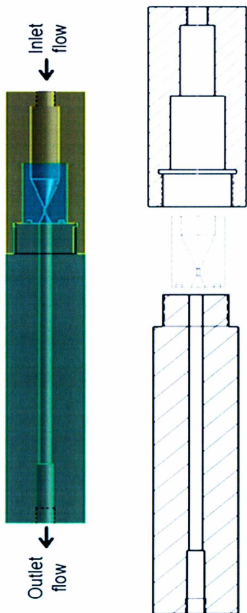


Figure 5.1 – Schematic view of the prototype design

The connections of the tools in the drill string are standard API threads; however, for laboratory convenience initial usage of the national pipe thread (NPT) was chosen. Nevertheless, design of the tool provides enough space to thread both ends to the API standard in the future, if needed. In case of future increase of orifice size, which is associated with field scenario usage, length and diameter of the outlet pipe should be increased as well, according to Pilipenko's paper [17]. In this situation, the outlet hole could be increased to an appropriate size and another section with API thread could be added to satisfy the length requirement.

All dimensions of the prototype parts can be found in the drawings, which are presented in Appendix B. Finally, based on these drawings, the prototype tool was manufactured at Memorial University's technical services machine shop (Figure 5.2). The tool was made from regular steel and its weight is 48 kg (106 lbs).

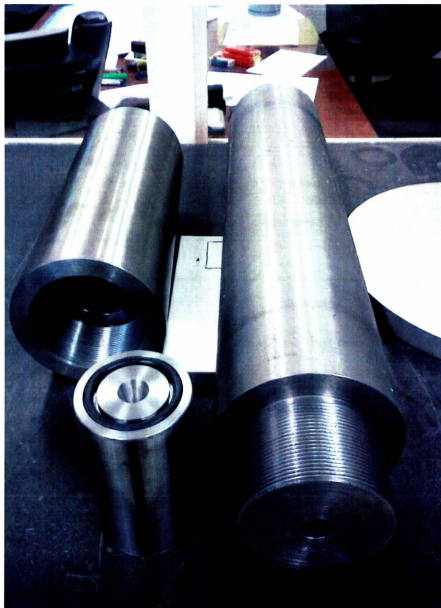


Figure 5.2 – Manufactured pulse-cavitation prototype

5.3 Experimental Setup

Apart from the prototype tool, another major component of the experimental system is a pump. The entire pump system was designed, purchased and built by the Advanced Drilling Group (ADG). The triplex reciprocating CAT pump is used in this system. Its specifications are provided in Table 5.5. Flow rate of the pump is controlled by a variable frequency drive (VFD). The system has double protection in order to avoid excessive pressure: a relief valve and an unloading valve. A pulsation dampener is located at the pump outlet and its pre-charged pressure is 450 psi.

Table 5.5 – Pump specifications

Parameter	Value	Dimension
Flow rate	5 - 40	USgpm
Pressure range	100 - 1000	psi
Rotary speed	680	rpm
Motor power	30	hp

Four measurement sensors were available during experimental investigation: a basic pressure gauge, two pressure transducers and an accelerometer. The pressure gauge was installed before the inlet hose; this was used to adjust the inlet pressure and to compare its value with inlet transducer readings. In order to measure vibrations of the prototype tool, a single axis accelerometer was used. Its maximum measurement range is $\pm 4g$ and maximum frequency output is 100 Hz. Flow rate was calculated from the VFD signal, which controls the pump motor speed.

Two pressure transducers were available for selection: the UNIK 5000 with a pressure range of 0 to 1000 psi, and the Cerabar PMP 131 with a pressure range of 0 to 1500 psi. Both sensors have high frequency response; however, we were limited to 1000 Hz of sampling frequency from the data acquisition system (DAQ). Both sensors have an output current of 4 to 20 mA. The UNIK 5000 was chosen as a sensor for outlet pressure because it is more sensitive: accuracy for both pressure transducers is $\pm 0.2\%$ of the full scale, but the full scale for UNIK is smaller, so it is more accurate.

Overall, during the presented experimental studies four measurements could be obtained (Figure 5.3): inlet pressure in a range of 0 to 1500 psi, outlet pressure in a range of 0 to 1000 psi, accelerations on the tool in a range of $\pm 4g$ and a flow rate within pump capabilities. These data were displayed during experiments in digital (data vs. time) and analog (gauge type) mode, as it is presented in the Figure 5.3.

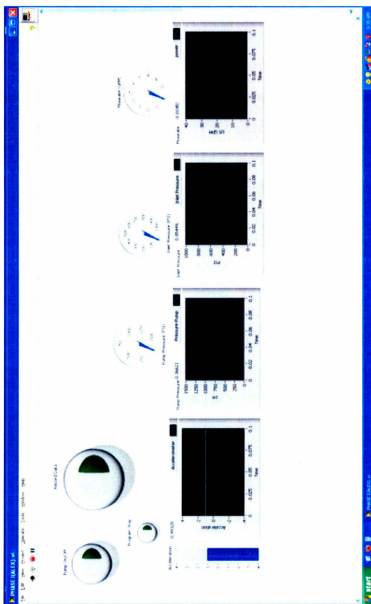


Figure 5.3 – Labview interface for the prototype experiments developed by Qian Gao

6 Prototype Experiments

This chapter will introduce experimental results of the pulse-cavitation prototype testing at the laboratory facilities. The purpose of the current experimental investigation is to confirm cavitation process initiation, to identify the operational limits of the tool and to characterize the pressure pulsations and vibration accelerations of the tool. The fluid used in these experiments was water.

6.1 Initial Experimental Observations

First trial runs were conducted as simply as possible. The main purpose of these runs was to achieve cavitation and to observe the behavior of the prototype.

Safety precautions were considered first. As stated previously, the tool can vibrate with very high accelerations, so it was decided to fix the tool. The prototype was placed on a steel “C” type beam to avoid its free rotation, which would occur on a flat surface. Cardboard was placed in between the tool and beam as a cushion material. A strapping belt was used to fix the prototype and beam with a wooden skid that was placed on the lab floor. Protective transparent screens were placed around the prototype in case of water splashes.

For the first runs no valves or transducers were used. Inlet and outlet hoses were connected to the tool through 1 inch nipples. The outlet hose was placed outside the lab, next to the drainage grate.

After all preparations were completed, the pump was started and the flow directed to the tool. During tool operation no leakages were observed, so protective screens were removed. The only factor that could be manipulated was flow rate. For the first trials it was decided not to go beyond 300 psi at the inlet pressure. This pressure was reached quite quickly, without a significant increase in flow rate. From the start of the tool operation, cavitation was detected by its distinguished noise and because of the presence of water bubbles in the outlet hose. Pressure pulsations were detected at the outlet of the tool; these could be easily sensed by touching the outlet hose. It was clearly identified that bubbles were collapsing in the hose and some of them were also observed at the hose outlet, next to the sewage grate. In spite of expectations, no significant vibrations were observed during the operation of the prototype.

Significant observations were made during the first trial runs with the pulse-cavitation prototype: cavitation did occur starting at small flow rates (6 gpm), pressure pulsations were generated at the tool outlet and no significant tool vibrations were observed. Also, considering the observations stated before, it was assumed that not all the bubbles collapsed inside the tool.

Despite the lack of vibrations, the first trial runs were considered successful, as cavitation was achieved and pressure pulses could be sensed at the tool outlet.

6.2 Characterization Tests

After initial observations of the performance of the prototype, it was decided to obtain pressure measurements at the outlet of the tool. In addition, two fittings were proposed to be installed at the same location.

A back pressure regulator was required to obtain a different ratio of outlet to inlet pressure. Furthermore, back pressure application was proposed as a solution to force cavities to collapse inside the tool. According to the available fittings selection at the laboratory, a ball valve was chosen as a back pressure regulator, rated for 1000 psi pressure with a 1 inch inside diameter. Although a ball valve might not be the best option for precise pressure regulation, it is the proper tool to create flow restriction. At this stage of the experiments we do not require very precise control of the back pressure.

A pressure transducer was installed on the 1 inch tee connecting the prototype and the ball valve. At this configuration we would be able to observe pressure pulsations caused by the tool at different inlet and outlet pressures. Two pressure transducers were available with pressure rates of 1000 and 1500 psi. It was decided to use a 1k transducer, as it is more sensitive.

Another fitting that was installed at the prototype outlet was a 5 foot long pipe with a 1 inch inside diameter. This idea was implemented to observe the difference in pressure pulsations right downstream of the prototype and at some distance. In addition, it was decided to observe if any vibrations would occur if bubbles collapsed inside the rigid pipe, which was connected to the tool.

Experiments were conducted following a simple procedure. The pump was running continuously during the experiment and the flow was directed to the pulse-cavitation prototype. The flow rate at the beginning was adjusted to 6 gpm, which corresponds to 100 psi of inlet pressure. While changing the flow rate, the pressure gauge was monitored to adjust required inlet pressure. At a certain setting of the tool, which corresponds to the adjusted inlet and back pressures, data were recorded for approximately 20 seconds. Within this time, measurements were taken every 0.001s, which provided a sufficient data set for future analysis.

The obtained data are presented in Tables 6.1 and 6.2. During experiments, significant vibrations were not observed in both cases: with a 5 foot long rigid pipe and without. In the case when the pipe was installed, bubbles were collapsing before they reached the outlet hose; nevertheless, this did not create significant vibrations on the tool body. However, some vibrations could be sensed on the prototype body, but they did not have enough amplitude to be obvious. In addition, these barely sensed vibrations occurred with and without the pipe.

Table 6.1 – Data obtained downstream of the 5 foot pipe

#	Flow rate, gpm	Inlet pressure	Outlet pressure	ΔP , psi	P2/P1	Max. P peak, psi	FFT analysis, Hz		
		P1, psi	P2, psi				Dom. f	2nd f	3rd f
1	6	100	15	85	0.15	300	10	60	125
2	6	100	25	75	0.25	350	10	60	125
3	6	100	40	60	0.40	330	10	60	125
4	6	210	170	40	0.81	880	10	125	240
5	8	200	15	185	0.08	300	2	125	240
6	8	200	25	175	0.13	480	2	125	240
7	8	200	35	165	0.18	440	12	125	240
8	8	400	300	100	0.75	1000	6	125	290
9	12	400	15	385	0.04	430	10	125	240
10	12	400	25	375	0.06	380	10	125	240
11	12	400	40	360	0.10	410	10	125	240

A pressure gauge was installed at the inlet side to observe inlet pressure. The flow rate estimation was displayed on the LabView interface; this was calibrated with a pump speed control knob. The average value of outlet pressure was used in these tables. Calculated values match the approximate average constant pressure that can be observed at the pressure plot (Figure 6.1). Another significant observation was regarding FFT analysis. The produced plot showed multiple peaks at certain frequencies. This is the reason for including the dominant frequency with the second and third frequency peaks. In addition, it was observed that inlet pressure remains constant, while back pressure fluctuates to some extent.

Table 6.2 – Data obtained directly downstream of the prototype

#	Flow rate, gpm	Inlet pressure P1, psi	Outlet pressure P2, psi	ΔP , psi	P2/P1	Max. P peak, psi	FFT analysis, Hz		
							Dom. f	2nd f	3rd f
1	6	100	15	85	0.15	380	3	125	240
2	6	100	15	85	0.15	420	3	125	240
3	6	100	25	75	0.25	370	10	125	240
4	6	210	175	35	0.83	890	10	125	240
5	8	200	15	185	0.08	375	3	125	240
6	8	200	15	185	0.08	340	125	3	240
7	8	200	25	175	0.13	520	125	240	3
8	8	400	350	50	0.88	1000	7	125	290
9	12	400	15	385	0.04	480	10	125	240
10	12	400	15	385	0.04	610	10	125	240
11	12	400	25	375	0.06	415	10	125	240
12	12	440	420	20	0.95	1000	10	125	90

As we can see from these two tables, maximum pressure peaks are in agreement as well as frequencies obtained from FFT analysis. It can be concluded that there is no significant difference in data readings obtained directly downstream of the prototype tool and 5 feet downstream from the tool. In addition, data shows that pressure pulsations are not damping within a few feet of the distance after the cavitation tool outlet.

Figure 6.1 presents the pressure plot for run number 8 from Table 6.2. As we can see, approximate average pressure is 350 psi. This value was also obtained by calculating the average data from all pressures. Significant pressure pulses that reach 1000 psi are clearly

visible in Figure 6.1. However, it is hard to distinguish the nature of the pulse, because the triplex pump has its own pulsations.

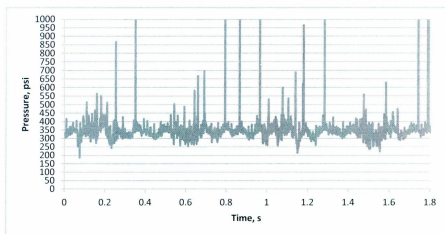


Figure 6.1 – Pressure pulses recorded directly downstream of the prototype

These results were quite promising. The first reason for this was that high amplitude pressure pulses were observed at the outlet of the tool. In addition, frequency peaks on FFT plots showed that pressure pulsations have some high frequency components, which are caused by cavitation.

The experiments were conducted at a maximum flow rate of 12 gpm, which corresponds to 400 psi inlet pressure. It was not possible to increase the inlet pressure with a flow rate increase during experimental runs. The reason for this was discovered after all runs were completed. The unloading valve at the pump outlet was set by default for the pressure of 450 psi. When we reached that pressure, the unloading valve opened and a portion of the water was by-passed to a water tank. After this problem was

identified, the unloader valve was adjusted for 850 psi to enable us to obtain data at higher pressures.

6.3 Prototype Performance Evaluation Experiments

After gaining some experience with tool operation and observing promising results described in the previous section, comprehensive experiments were conducted. At this stage of experimental investigation it was decided to conduct tests over the available pressure range, reaching a maximum value of 800 psi (the unloader valve was set for 850 psi for safety reasons). Furthermore, in order to monitor pressure pulsations at the tool inlet, a 1500 psi Cerobar pressure transducer was installed at the inlet side. As mentioned before, some vibrations were sensed on the tool body, therefore, a uni-axis accelerometer was attached on the tool to obtain axial vibration measurements. As in the previous case, a 1000 psi pressure transducer with higher accuracy was installed at the tool outlet.

Figure 6.2 presents photos of the experimental setup. Unlike the previous experiments, the tool in the “C” type beam was placed on the cart to provide more flexibility for vibration observations (Figure 6.2 a). Previously it was placed on the wooden skid. The pump system was connected to the tool by a flexible hose; a pressure transducer on the T connection was installed upstream of the tool (Figure 6.2 b). An accelerometer with another pressure transducer was installed at the outlet (Figure 6.2 c), followed by a ball valve as a back pressure regulator. Flexible hose connected to the ball valve directed water to the drainage grate.



a



b



c

Figure 6.2 – Experimental setup: (a) overall view, (b) inlet, (c) outlet

All the tests were conducted successfully and the results are in Appendix C. Data were obtained for an inlet pressure range from 100 to 800 psi with a 100 psi increment. For every inlet pressure, 6 data points were obtained for various back pressures, starting from the fully opened ball valve to the almost closed one. Overall 48 data sets were available for the analysis.

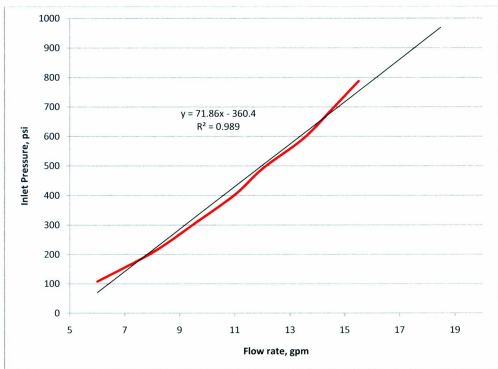
Maximum considered inlet pressure was achieved at the flow rate of 15.5 gpm. Flow rate versus inlet pressure plot is presented in Figure 6.3. As we can see, inlet pressure is proportional to flow rate and the slope is quite steep. Maximum pump pressure could be reached at 19 gpm, which is basically half of the pump flow rate capability. These results can be compared to calculations performed in Section 5.1. Three methods were used to estimate pressure drop across the orifice and the results are presented in the Tables 5.2, 5.3 and 5.4. Data from Table 5.2 do not correspond to experimental observation, so the assumption about its poor accuracy was correct. The second method of calculations is closer to the actual data, as the estimated pressure drop at 15 gpm was 1105 psi. However, it is still not accurate enough. The best fit showed the equation obtained from paper [17]. At a constant orifice diameter with a variable flow coefficient, 800 psi pressure drop was estimated at 16.7 gpm for the flow coefficient of 0.8, and at 14.6 gpm for the flow coefficient 0.7. These data were extrapolated and the flow coefficient for the pulse-cavitation prototype was estimated as 0.75.

Pressure pulses pattern can be subdivided for low (100 – 300 psi) and high pressures (above 300 psi). At low pressures (Figure 6.4) outlet pressure pulses regularly exceeded inlet pressure. This pattern is the same for the fully opened and partly closed ball valve.

From Figure 6.4 it is visible that some peaks reached 1000 psi, which is 5 times higher than inlet pressure (200 psi).

The pulsation profile looks different for high inlet pressures. Figure 6.5 presents pulsations for test run #46 with a $P2/P1$ ratio of 0.07, which means that back pressure is not high (53 psi). Figure 6.6 shows the pulsation pattern for test run #48. Both runs are conducted at 800 psi, but the second one has $P2/P1$ ratio of 0.7, and back pressure in this case is 551 psi.

As we can see from these figures, pressure pulsations are much more intense for run #48. At a small outlet pressure we can see significant pressure pulses; however, the difference between inlet and outlet pressure is big, so outlet pressure pulses are barely exceeding the inlet pressure. At low pressures the difference is not that big, so outlet pressure peaks can still exceed inlet pressure. Nevertheless, when the ball valve restricts the flow downstream of the tool, creating significant back pressure, we can see that outlet pressure pulses become more intense and they exceed inlet pressure often (Figure 6.6).



a

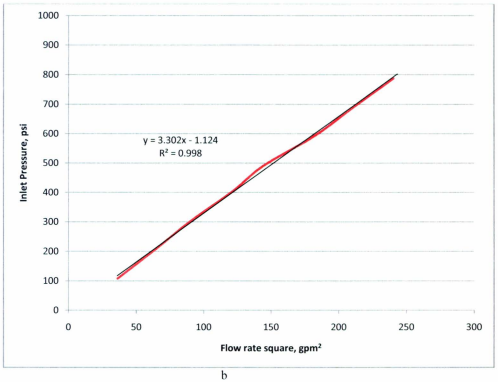


Figure 6.3 – Inlet pressure versus flow rate: (a) P vs. Q, (b) P vs. Q²

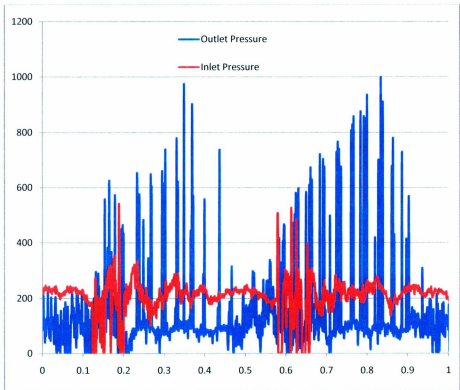


Figure 6.4 – Pressure pulsations for test run #11

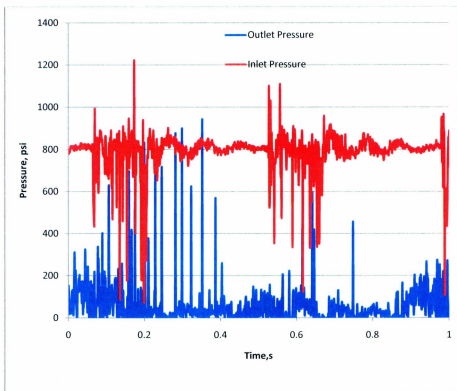


Figure 6.5 - Pressure pulsations for test run #46

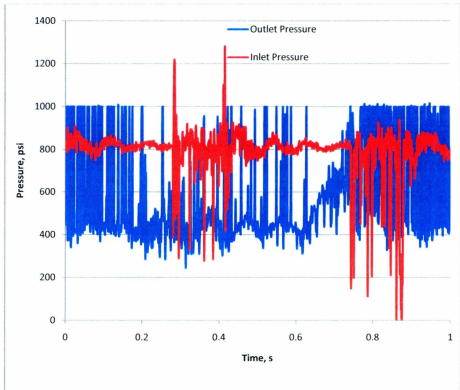


Figure 6.6 - Pressure pulsations for test run #48

As a result, we can conclude that outlet pressure pulsations are stronger and more intensive with higher back pressure. In a real case scenario, there will always be a significant amount of back pressure due to bit nozzles and wellbore frictional pressure losses, as well as hydrostatic pressure in the annulus. Consequently, we can assume that pressure pulsations would be at a higher rate in drilling field conditions.

The vibration accelerations example is presented in Figure 6.7. The pattern of vibration accelerations is similar for all runs. The saturated range of vibrations is always within -0.5 to +0.5 g. In addition, high peaks reach values up to 4.48g. However, the

maximum measurement range is ± 4 g, according to specs, so values above the range are not reliable. Nevertheless, in the results we can see few maximum acceleration values that exceed acceleration of 4g. The majority of maximum acceleration values are within the range of 2 to 4 g.

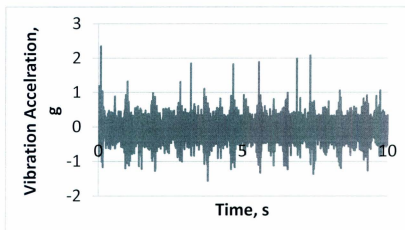
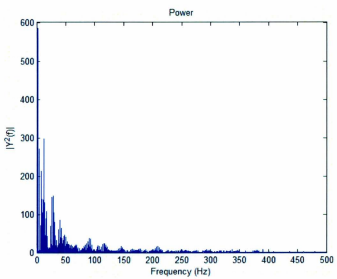
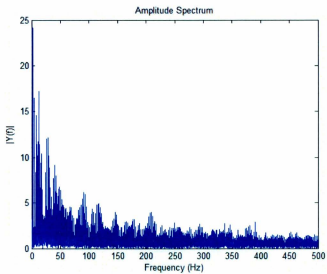
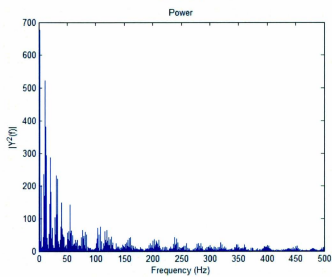
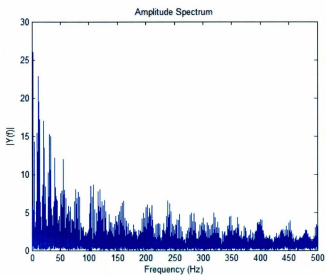


Figure 6.7 – Vibration acceleration plot for test run #46

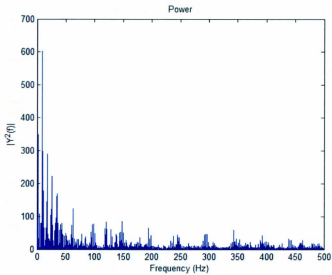
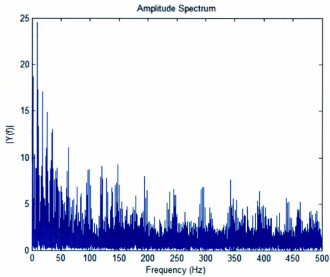
FFT analysis was applied to the pressure and vibration measurement data to compare and evaluate them. First of all, it was observed that at the inlet side of the tool, low frequency pressure pulsations are always dominant (Figure 6.8). These plots correspond to test runs #15 at 300 psi (Figure 6.8 a), #27 at 500 psi (Figure 6.8 b) and #40 at 700 psi (Figure 6.8 c). As shown, for all pressure ranges, dominant frequencies are within the range of 1 to 15 Hz. Furthermore, after the dominant frequency peak, the amplitude on the FFT plot sharply decreases. Therefore, we can conclude that no significant high frequency pulsations occur at the inlet side of the pulse-cavitation prototype tool.



a



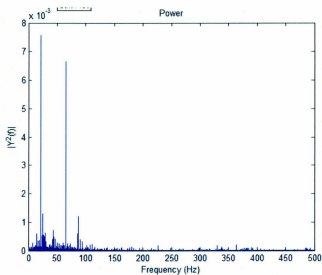
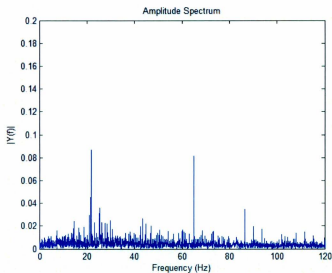
b



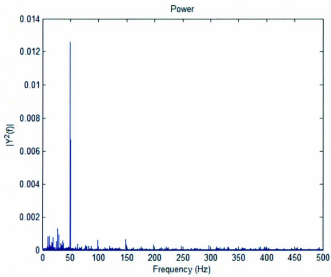
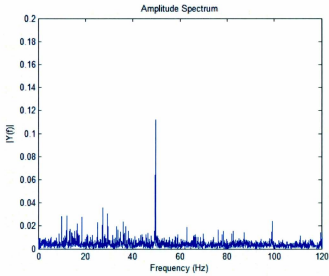
c

Figure 6.8 – FFT plots of amplitude and power spectrum for inlet pressure pulsations: (a) run #15, (b) run #27, (c) run #40

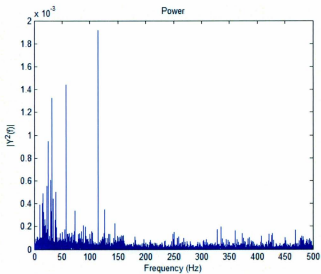
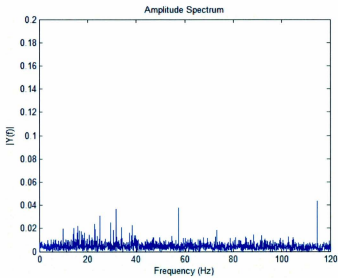
Vibration acceleration data showed clear peaks (Figure 6.9).



a



b



c

Figure 6.9 – FFT plots of amplitude and power spectrum for acceleration vibrations: (a) run #4, (b) run #35, (c) run #46

Three major patterns for acceleration data were observed. The most common one had two dominant frequency peaks, for instance test run #4 at 100 psi (Figure 6.9 a). Another case was associated with a single distinguished frequency peak, similar to test run #35 at 600 psi (Figure 6.9 b). Sometimes low frequency noise was observed on the FFT plot, as for test run #46 at 800 psi (Figure 6.9 c), however, this is the less common trend that was observed during FFT analysis.

The most interesting observations were made while analyzing outlet pressure pulsations (Figure 6.10). First of all, we can see clearly distinguished multiple peaks at various frequencies. Unfortunately, the limit of current FFT analysis is 500 Hz, (sampling rate was 0.001 s), because Nyquist frequency equals half of the sampling frequency. Nevertheless, it seems that dominant frequency peaks are always below 500 Hz.

Another significant observation that was made is the period of the multiple frequency peaks. From Figure 6.11 it is obvious that the frequency of a second peak is twice as large as the first peak. This phenomenon is observed throughout all FFT plots for outlet pressure pulsations. Figure 6.11 shows test run #38 at full FFT scale (Figure 6.11 a) and enlarged scale at the first and second peak (Figure 6.11 b). As we can see, the first peak occurs at a frequency of 53.5 Hz, and the second one at 107 Hz. From this we can conclude that multiple peaks are periodical, and that the period is equal to the first peak.

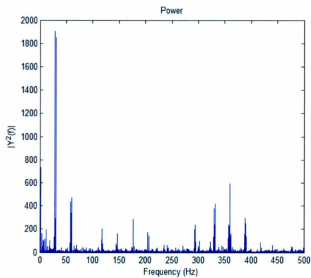
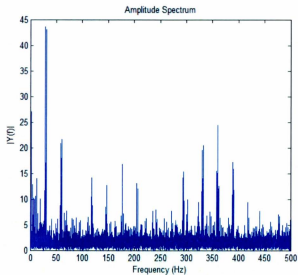
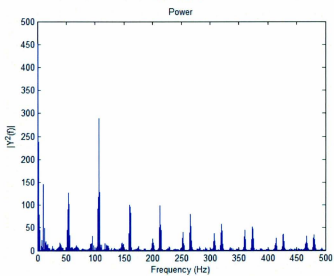
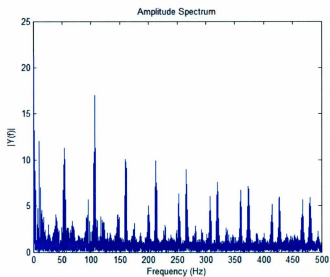
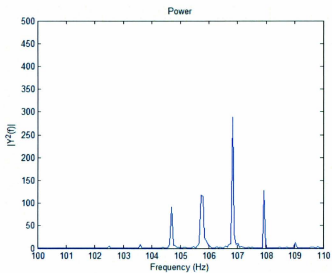
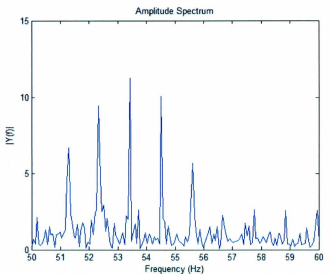


Figure 6.10 – FFT plot of amplitude and power spectrum for outlet pressure (test run #11)



a



b

Figure 6.11 – FFT plot for outlet pressure (test run #38): (a) full scale, (b) enlarged peaks

The phenomenon described above is not typical of reflected waves. In this case the frequency shift should be equal to the sound speed divided by two lengths of the tool. However, in such a scenario the frequency shift would be constant, because of the constant tool geometry. As observed from the FFT plots, the frequency shift is equal to that of the first peak. After consultations and some literature review, this phenomenon was explained as non-linear harmonic behaviour: sub- and superharmonic.

According to [37], liquid that contains microbubbles produces a nonlinear response that results in harmonic dispersion. This produces harmonics with multiple frequencies (superharmonics and subharmonics). Lauterborn [38] conducted a study in nonlinear oscillations of gas bubbles in liquids. According to his observations, the cavitation bubble, with its linear resonance frequency of ν_0 , was influenced by the sound field with the frequency of ν and this resulted in multiple resonance peaks, which were identified as super and subharmonic (Figure 6.12). In this Figure “normalized” amplitude is plotted as a function of “normalized” frequency, where R_n is bubble radius and R_{max} is maximum radius of a bubble [38]. It is clearly shown that the main resonance occurs in the region $\nu/\nu_0=1$ and distinguished resonances occur at the following peaks.

In addition to this, the study described in [39] also states that multiple harmonic resonances were observed for the cavitation bubble affected by acoustic signals. The authors also observed that superharmonics can reach up to the 20th order.

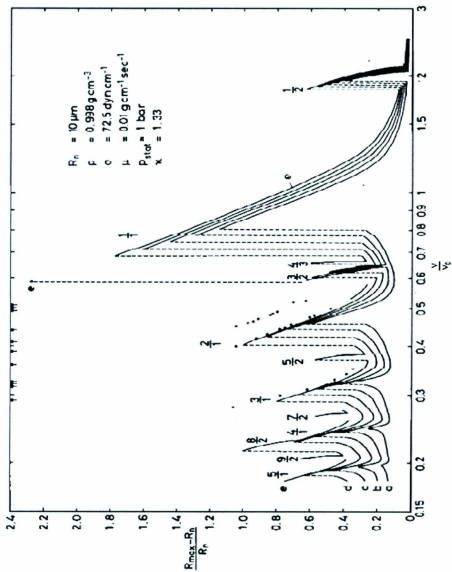
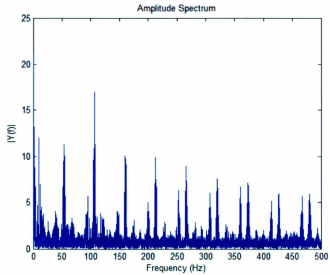


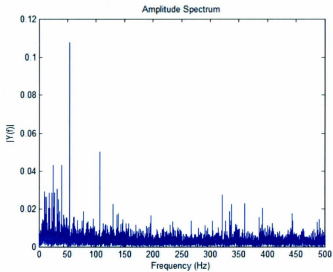
Figure 6.12 – Frequency response curves [38]

From the reviewed papers, it was concluded that the cavitation process that occurred during the prototype operation is classified as nonlinear harmonic behaviour. This explains the multiple peaks on the FFT plot and confirms that high frequency pressure pulses that were observed are due to the collapse of cavitation bubbles.

The FFT analyses for vibration accelerations and pressure pulsations were compared. First of all, from Appendix C we can see that vibration frequency very often matches pressure pulsation frequency. However, sometimes a second or other pressure peak is dominant, but vibrations still occur at the frequency of the first outlet pressure peak (Figure 6.13). As we can see from Figure 6.13, a second peak of outlet pressure pulsations is dominant at approximately 100 Hz. Nevertheless, Figure 6.13 b presents FFT analysis of vibration accelerations for the same test run, and we can see that the dominant frequency matches the first frequency peak of the pressure pulsations. However, we can still observe a significant peak on the vibration FFT plot at 100 Hz. The only time when vibrations occurred at the second pressure pulsation peak was in test run #46 (Appendix C). The recorded acceleration frequency was 116 Hz, while the first pressure pulsation frequency was 58 Hz. However, according to accelerometer specs maximum frequency response is 100 Hz, which means that at a higher frequency, amplitude measurements are not reliable, but frequency measurement should be reliable. Even though we can clearly observe that vibrations occur due to pressure pulsations at the outlet, as their frequency matches, it should be also possible to vibrate at the second or other peaks, if they become significantly dominant.



a



b

Figure 6.13 – Frequency of (a) pressure pulsations and (b) vibration accelerations

Figure 6.14 presents the vibration frequency dependence on the prototype inlet pressure. As we can see, these parameters are proportional, and an increase in inlet pressure leads to an increase of the vibration frequency. The lines presented on the plot show vibration frequencies that occur in the first frequency peak of the pressure pulsations (observed during experiments) and may occur in the second one (assumed to be possible). Considering the 1000 psi inlet pressure, prototype should vibrate at a frequency of 70 Hz; if it were possible to “shift” vibrations to the second pressure pulsation frequency peak, we could have achieved 140 Hz.

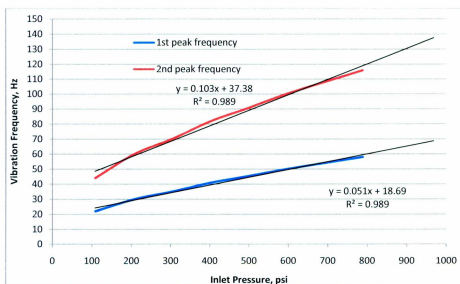


Figure 6.14 – Vibration frequencies versus inlet pressure

6.4 Confirmation Tests

Experimental results presented in the previous section showed some trends and proved the concept capability. However, there are still a few questions left after analysis was conducted. First of all, within 6 experimental measurements at a constant inlet pressure we did not have enough data points to observe a P2/P1 ratio influence on the prototype performance. Secondly, measurement questions were raised due to accelerometer measurements, which sometimes exceeded the measuring range stated in the specification. In addition, pressure pulsations caused by the pump should be distinguished more clearly.

The first experiments that were conducted aimed to observe a P2/P1 ratio influence. According to Manko [17], with the ratio increase we should observe a frequency increase, and a decrease in outlet pressure pulsations and vibration accelerations. The test was designed to operate the prototype at three inlet pressures: 300, 500 and 700 psi. However, during operation of the tool at 500 psi, the outlet pressure transducer was damaged. During the entire operation of the tool, outlet pressure pulsations were exceeding 1000 psi, which is the measuring limit of the transducer. It was assumed that the transducer was damaged due to continuous exposure to high pressure pulses. Nevertheless, all 12 data points were obtained for an inlet pressure of 300 psi (Appendix D), which is enough to characterize a P2/P1 ratio influence. Further experiments were not conducted in order to avoid damage of other pressure transducers, which are also rated for 1000 psi.

During analysis of the experimental results the same trends were observed as for previous experiments. First of all, vibration and pressure pulse frequencies matched those

of previous experiments. Pressure pulsations at the outlet were reaching 1000 psi, which is more than 3 times higher than inlet pressure.

During FFT analysis of 12 points with different P2/P1 ratios, no frequency change was observed. It seems that vibration frequency depends only on the inlet pressure, for this prototype (Figure 6.15).

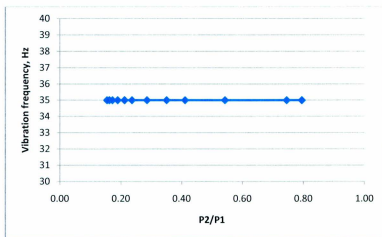


Figure 6.15 – Vibration frequency versus P2/P1 ratio

Vibration accelerations should be maximum at a P2/P1 ratio, close to 0.2, and then steeply decrease. From Figure 6.16 it seems that maximum accelerations were achieved within the ratio range of 0.15 to 0.2, but we cannot observe a clear pattern.

It was not possible to characterize pressure pulsation magnitude due to the measurement limit of 1000 psi, which was exceeded quite often.

Another significant feature of the prototype operation was observed. As we can see from the results (Appendix D), inlet pressure remains constant in the approximate ratio

range from 0.15 to 0.7. After reaching the ratio of 0.7, inlet pressure starts to build up with an increase of the back pressure.

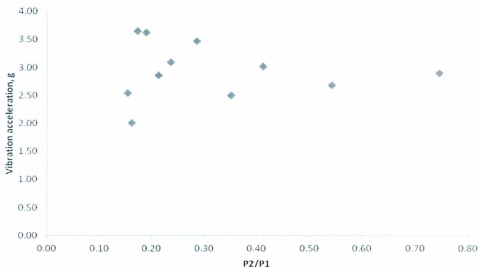


Figure 6.16 - Vibration amplitude versus P2/P1 ratio

The next step was to evaluate noise of the measurement tools and estimate its possible influence on the experimental results.

In order to characterize pressure pulsations and monitor the noise in the pressure transducer signal, a simple test was conducted. An inlet hose was connected to the outlet through a 1 inch tee with a 1500 psi Cerobar pressure transducer. Another 1000 psi pressure transducer (with similar characteristics to the damaged sensor) was attached to a port on the other component which was opened to the atmosphere. Measurements were obtained starting from the flow rate of 8 gpm.

Pressure pulsations caused by the pump were calculated first. According to the specification, the speed of the pump at the full flow rate of 40 gpm is 680 rpm. For the

triplex pump (with three pistons) three strokes take place during a single rotation of the pump pulley. Then maximum frequency that the pump can produce is 34 Hz. According to the manual, the pump speed is proportional to the flow rate, therefore, the frequency can be calculated for any specific flow rate. At the same time frequency peaks from the data were analyzed. Calculated values and FFT peaks from pressure transducer measurements are plotted in Figure 6.17.

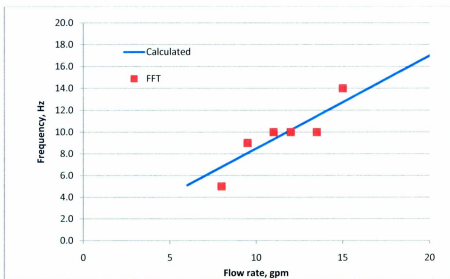
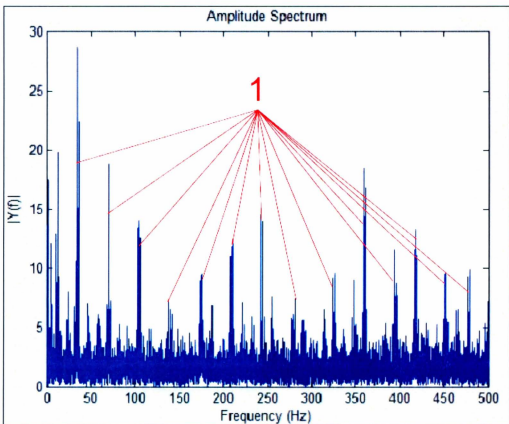


Figure 6.17 – Pump pressure pulsations

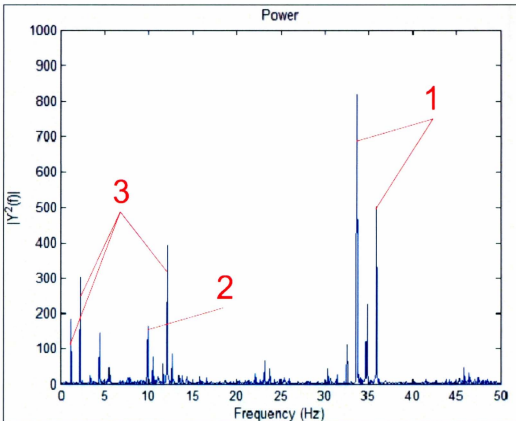
The FFT data is slightly scattered due to pressure transducer noise, however, the calculated pulsation frequency corresponds to the actual data. As we can see, the maximum frequency caused by the pump in the considered flow rate range is from 4 to 15 Hz. This means that observed pressure pulsations at the outlet of the tool, which are in the range of 25 to 400 Hz are due to cavitation.

Both pressure transducers have some noise. Even the 1000 psi transducer that was not attached to the flow system showed some small pulsations. It was observed that for both measurements, sensor noise has two constant frequency peaks on the FFT plot, 2 Hz and 12 Hz. These frequencies are smaller than the pulsations created by cavitation; in addition, the amplitude on the FFT plot for the detached 1000 psi transducer is smaller than that observed for previous experiments. The magnitude of the average pressure recorded by the detached transducer showed a constant pressure, within 4 to 5 psi. Furthermore, no multiple peaks or similar trends were observed on noise FFT plots, so recorded pulsations were not due to transducer noise. Overall it was concluded that noise of the pressure transducer could not significantly affect the results.

These additional experiments confirm the previous suggestion about the low frequency component of the pump pulsations on the outlet pressure FFT plots. Figure 6.18 presents the FFT plot of the outlet pressure for confirmation run #8 (Appendix D). In this figure, the amplitude plot has an entire range of 500 Hz and a power plot range limited to 50 Hz, in order to present low frequency components more clearly. From Figure 6.18 we can clearly identify pressure pulsations caused by cavitation (1) with the frequency peaks starting from 35 Hz. The low frequency range consists of two components: pump pulsations (2) and noise (3), which corresponds to the 2 and 12 Hz noise for pressure transducers mentioned above. Pressure pulsations caused by the pump were estimated at 8.1 Hz by numerical method and on FFT we can observe approximately 9.5 Hz.



a



b

Figure 6.18 – FFT description of pressure pulsations caused by: 1- cavitation, 2- pump pulsations, 3 - noise

During the pump pulsation experiment, an accelerometer was placed on the rig that was located next to the pump. It was noticed that the accelerometer had significant noise during operation of the pump. The plotted vibration accelerations look similar to those in Figure 6.7, which was recorded for previous experiments. The magnitude of the maximum acceleration peaks reached up to 3.5g, in addition, on FFT plots some high

frequency peaks were present as well. From this we can conclude that the magnitude of the acceleration vibrations recorded during previous tests might not be reliable due to accelerometer noise. However, as the frequency of the vibration accelerations matched the frequency of pressure pulsations, it was assumed that these data were correct. After this analysis, the VARD group concluded that the current accelerometer is not the best option for future vibration measurements and subsequent tests would use high frequency response accelerometers.

Another observation was made while the pump was not in operation. In this case the noise for the pressure transducers and accelerometer become negligible and the FFT plot was clear, without any peaks. This brought the assumption that pump frame vibrations might be transferred to the rig, so this could affect the accelerometer noise described above.

One more observation was done during the experimental study. As was expected, rust appeared on the tool interior (Figure 6.19 a) and exterior (Figure 6.19 b) surfaces, because the prototype body was manufactured from regular steel. However, this did not have an influence on the outcome results. First of all, rust appeared after the first trial tests. Secondly, confirmation experiments were conducted one week after full experiments and the same agreed data was produced. Rust influence was neglected at the design stage. The reason is that rust can only affect the interior surface and increase wall roughness that corresponds to frictional pressure losses. However, in our case frictional losses downstream of the cavitating part could be neglected because they are too small in comparison to shock losses in the orifice. Consequently, prototype performance mainly depends on the shock pressure loss, which is not dependent on the surface roughness.

Rust could only cause a difference in the tool performance if it changed the diameter of the orifice, which would influence inlet pressure response with the flow rate and consequently the frequency response of the tool. After analyzing surfaces, an orifice diameter increase was not observed; this could be also concluded from experimental results.

The cavitating part had almost no rust on the exterior, which means that the o-ring restricted flow around the part. Flow passage downstream of the pipe was inspected and no significant rust voids or serious damage were observed. Major rust was observed upstream (Figure 6.19c) of the orifice. This is caused by the significant amount of water that remained at the inlet side during the non-operational time of the tool.

In conclusion, from the confirmation experiment's outcomes, it can be said that results are quite consistent and that at the adjusted inlet pressure we have constant and predictable frequency of the pressure pulsations and vibration accelerations. In addition, it was confirmed that pressure pulsations caused by the pump are of a low frequency, and could not interfere with the recorded higher frequency pressure pulsations. From the information presented above, there is no doubt that the pressure transducer noise could be misinterpreted in the reported results, however, the accelerometer measurement has some doubt, and especially the magnitude of the accelerations, and this should be confirmed in future experiments with another approach to vibration measurement.



a



b



c

Figure 6.19 – Rust observation on the prototype surfaces: (a) orifice, (b) exterior, (c) inlet

7 Conclusions and Future Work

7.1 Conclusions

This study was intended to develop a potential tool for vibration assisted drilling experiments. The tool is required to apply vibrations on top of the bit and its geometry should fit the drill string sub in order to be feasible for a real field drilling scenario. In addition, the prototype should have a simple controlling mechanism driven by hydraulics (drilling mud) to avoid other energy sources downhole.

A potential candidate was considered among studied and proven technologies. As a result, the cavitation tool concept was chosen for prototype development, due to its main advantages, such as simple design, and the absence of mechanical rotating parts and springs, as well as not having parts with a high wear rate. These factors, along with proposed performance characteristics observed by other researchers, made a major contribution to the potential prototype choice. As the result, a cavitation phenomenon was chosen as an approach to create a vibration oscillation tool. The other part of the investigation was divided into three major stages: numerical simulations, engineering design and experimental confirmation. First, the flow passage, which is critical for the proposed tool, was chosen in advance and was simulated with CFD software. Simulations yielded promising results that were partially in agreement with referenced studies. After the numerical suggestion of tool feasibility, a prototype was designed with the same flow passage that was simulated. The tool design included laboratory capabilities and

requirements for possible future field installation with a 6 inch bit. After the tool was manufactured, experimental investigation was conducted.

As a result of the experiments, major performance observations were reported:

- cavitation occurred over the entire tested pressure range, 100 to 800 psi;
- inlet pressure pulsation was mainly caused by low frequency pump pulsations;
- cavitation created pressure pulsations, which caused vibrations on the tool. This can be concluded from a match of the dominant frequencies of pressure pulses and vibration accelerations. In addition, these frequencies were high enough to distinguish them from pulsations caused by the pump;
- outlet pressure pulse peaks exceeded inlet pressure by 3 to 5 times. In addition, it was concluded that pulsations are more intense when back pressure is higher;
- outlet pressure pulsations had multiple resonance frequency peaks due to the nonlinear harmonic nature of cavitation bubble behaviour;
- vibrations occurring at the frequency of outlet pressure pulsations caused by cavitation and its frequency matched the first frequency peak of pressure pulsations; however, it was assumed that vibrations can occur at the second and other peaks;
- at the current stage of prototype development vibration frequency is dependent only on the prototype inlet pressure;
- the amount of pressure drop across the pulse-cavitation prototype can be controlled by back pressure, however, in order to maintain constant inlet pressure, at least 30% of the pressure should be dropped ($P_2/P_{1max}=0.7$).

Experimental and simulation results were compared and the conclusion has been made that the existing CFD model mainly can be used to predict cavitation initiation. In addition, experiments confirmed two simulation observations: frequency of pressure pulsations increases with an inlet pressure increase, and outlet pressure peaks can exceed inlet pressure. However, the simulated frequency response of outlet pressure pulses does not agree with experimental data, probably due to boundary conditions of the simulated model.

The overall outcome of this entire investigation can be concluded as quite successful, because the initial goal was achieved: the tool can produce vibrations, it has a simple design suitable for field drill string installation, and drilling mud is the only supply source that is required for prototype operation. In addition, the pulse-cavitation prototype produces significant outlet pressure pulses, which can exceed inlet pressure. These partially confirm results and theory presented in Pilipenko study [17]. Nevertheless, at this stage of prototype development relatively small frequencies were obtained. In addition, the current experimental setup did not allow the creation of a considerable vibration amplitude, and acceleration magnitude measurements were not consistent, taking into account the noise in the measurement device. Considering these points, we can conclude that initial development confirmed the feasibility of the prototype and further development is encouraged.

7.2 Future Work

Considering results obtained during this investigation, some goals for future prototype development can be proposed:

1. Tool operation confirmation with: According to the simulations, a prototype tool should have a similar performance to viscous fluids, but its performance can differ in terms of frequency response and outlet pressure peak magnitudes. This experimental confirmation has the first priority due to the fact that all drilling operations are performed with drilling mud of high viscosity, including thixotropic features.
2. Geometry improvement: As was reported in referenced studies and observed during experiments, flow passage is one of the most important factors of the prototype performance. Consequently, improving geometry of the hydraulic passage can improve tool performance to the required parameters. This improvement can be conducted by optimizing inlet and outlet geometrical parameters (inlet and outlet angle of the cavitating part, length of the orifice, length of the outlet pipe and others) as well as by adding new components or elements up- or downstream of the orifice.
3. Experimental frame development: In order to create vibration amplitude and measure accurately vibration accelerations and forces that can be applied by the prototype tool, an experimental frame should be designed. This should provide controlled compliance and accurate measurements of the vibrations.

4. Field test experiments: After performing previously mentioned development stages, a field test should be conducted. First of all, the prototype tool should be modified in order to work with flow rates that are appropriate for real drilling conditions (this feature was considered during the design stage). Secondly, real drilling mud should be used during experiments to observe viscosity and solid content influence on the tool performance and lifetime. In addition, field experiments are required in order to gain experience of the tool operation in the downhole, and to monitor bottom hole pressure change during tool operation and vibration propagation in the drill string.

Bibliography

- [1] BP Energy Outlook 2030: January 2012 (n.d). *BP Global*. Retrieved from <http://www.bp.com/energyoutlook2030>.
- [2] Offshore Rig Day Rates (n.d.). Retrieved from <http://www.rigzone.com/data/dayrates/>.
- [3] Garnier A.J., van Lingen N.H. (1959) Phenomena Affecting Drilling Rates at Depth. *Petroleum Transactions*, 216, 232-239.
- [4] Pennington J.V. (1953) Some results of DRI Investigations – Rock Failure in Percussion. *Drilling and Production Practice*, API 53-32.
- [5] Li H., Butt S., Munaswamy K., Farid A., Memorial University of Newfoundland (2010). Experimental Investigation of Bit Vibration On Rotary Drilling Penetration Rate. *44th U.S. Rock Mechanics Symposium and 5th U.S.-Canada Rock Mechanics Symposium*, 6.
- [6] Li. H. (2011) Experimental Investigation of the Rate of Penetration of Vibration Assisted Rotary Drilling (Master's Thesis). Memorial University of Newfoundland, St. John's.
- [7] Babatunde Y., Butt S., Molgaard J., Arvani F., Memorial University of Newfoundland (2011). Investigation of the Effects of Vibration Frequency On Rotary Drilling Penetration Rate Using Diamond Drag Bit. *45th U.S. Rock Mechanics / Geomechanics Symposium*, 6.

- [8] Babatunde, Y. (2011) The Effects of Varying Vibration Frequency and Amplitude for VARD Drilling Optimization (Master's Thesis). Memorial University of Newfoundland, St. John's.
- [9] Pixton D., Hall D. (2010). A New Generation Mud-Hammer Drilling Tool. *Annual Report by Novatek Inc.*
- [10] Kolle J. (2004) Hidropulse Drilling. Final report, 28.
- [11] Kolle J. (2004) Hydraulic Pulse Drilling. *GTI Natural Gas Technologies II Conference*, 14.
- [12] Li G., Shi H., Liao, H., Shen, Z., Niu, J., Huang, Z., Luo, H. (2009) Hydraulic pulsed cavitating jet-assisted drilling. *Petroleum Science and Technology* 27(2), 197-207.
- [13] Li G., Shi H., Niu J., Huang Z., Tian S., and Song X., China University of Petroleum, Beijing (2010). Hydraulic Pulsed Cavitating Jet Assisted Deep Drilling: An Approach to Improve Rate of Penetration. *International Oil and Gas Conference and Exhibition in China*. doi: 10.2118/130829-MS.
- [14] National Oilwell Varco (2009). Technical Summary. In National Oilwell Varco. Retrieved from http://www.nov.com/Downhole/Drilling_Tools/Drilling_Agitor/Agitor_Tool.aspx?terms=agitor.
- [15] McGill H. L., Johnston Testers; Dalton C., U. of Houston (1968) Analytical and Experimental Investigation of Flow in a Hydraulic Jar. *SPE Journal* 8(4), 351-358.
- [16] Massner P.F., Stang D.L. (2001) Hydraulic Drilling Jar. *U.S. Patent No. 6,263,986 B1*. Washington, DC: U.S. Patent and Trademark.

- [17] Manko I.K., Pilipenko V.V., Zapols'ky L.G. (2003) Use hydrodynamic cavitation for increase of efficiency of process of well drilling. *Fifth International Symposium on Cavitation*, 7.
- [18] Pilipenko V.V., Manko I.K., Zapols'ky L.G., Dolgoplov S.I., Nikolaev O.D. (2005) High-Frequency downhole hydrovibrator for enhancing the effectiveness of drilling in hard and super hard formations. *AADE National Technical Conference and Exhibition*, 8.
- [19] Pilipenko V.V., Manko I.K., Dolgoplov S.I., Nikolayev O.D. (2006). Effect of liquid flowrate on longitudinal vibration acceleration parameters of a cavitation hydrovibrator (in Russian). *Naukovy Vistnyk NDU* 2, 36-39.
- [20] Bakker T. W., Vladimir I. I. (2002). Cavitator for Effective Well Cleaning. *SPE/ICoTA Coiled Tubing Conference and Exhibition*. doi: 10.2118/75352-MS.
- [21] Angona F. A. (1974) Cavitation, a Novel Drilling Concept. *International Journal of Rock Mechanics and Mining Sciences* 11(4), 115-119.
- [22] Jones I. R., Edwards D. H. (1960). An Experimental Study of the Forces Generated by the Collapse of Transient Cavities in Water. *Journal of Fluid Mechanics* 7, 596 – 609.
- [23] Collins English Dictionary (2009). Dictionary.com. Retrieved from <http://dictionary.reference.com/browse/schlieren>
- [24] Xiao G., Zhimin D., Southwest Petroleum Inst.; Li G., Shengli Oilfield; Shu Z., Dianqiangui Oilfield. (2004) High Frequency Vibration Recovery Enhancement Technology in the Heavy Oil Fields of China. *SPE International*

Thermal Operations and Heavy Oil Symposium and Western Regional Meeting. doi: 10.2118/86956-MS.

[25] Harthy A., Petroleum Development Oman; Abdulkadir R., Halliburton; Sipra I., Saeb J., Raiturkar A., Petroleum Development Oman; Bailey M., Venditto J., Halliburton. (2004). Screen and Near-Wellbore Cleaning and Stimulation Tools Evaluation: Recent Experience in Well Operation. *SPE/ICoTA Coiled Tubing Conference and Exhibition*. doi: 10.2118/89653-MS.

[26] Bakulin V., Geotechnologies. (2003) Novel Method And Equipment of Oil Extraction Using Seismic Stimulation And Cavitation. *2003 SEG Annual Meeting. 4*.

[27] Gorbachev Y.I., Kuznetsov O.L., Rafikov R.S., Pechkov A.A. (1998) Physical foundations of acoustic methods of reservoir stimulation. *Geophysica* (in Russian) (4), 5-9.

[28] Kardysh V.G., Kiselev A.T., Melamed Y.A. (1989) Hydropercussion drilling using roller drill bits. (in Russian). *Novel Facilities for Exploration Drilling* (6), 91-98.

[29] Volkov S.A., Sulashkin S.S., Anreev I.I. (1965) Vibration method of rock destruction (in Russian). *Burovoe delo*.

[30] Manko I.K. (1977) Effect of the diffuser angle of a Venturi tube on the frequency and maximum pressure of high-frequency cavitation oscillations (in Russian). *Naukova Dumka*, 34-38.

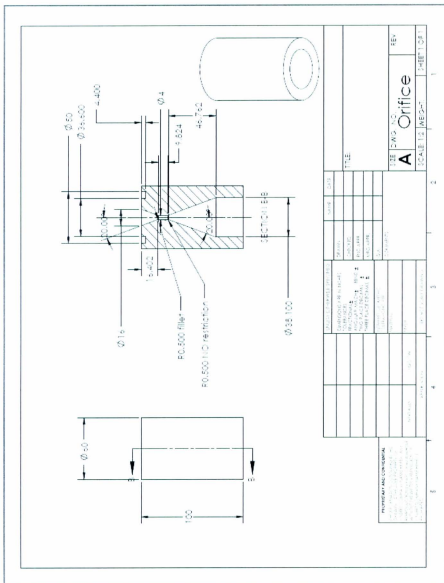
[31] Pilipenko V.V. (1989) Cavitation self-oscillations (in Russian). *Naukova Dumka*, 316.

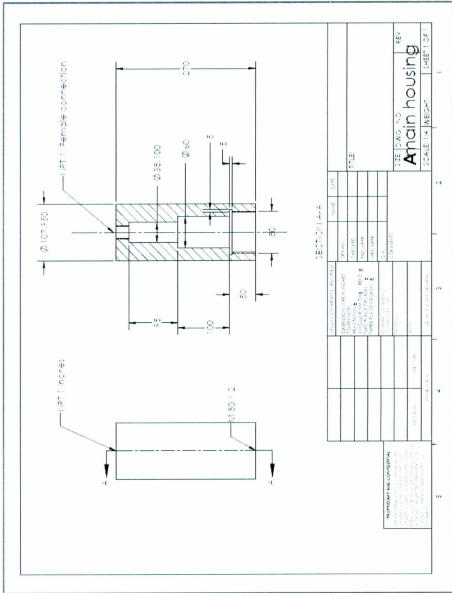
- [32] Growcock F., Harvey T. (2005). *Drilling Fluid Processing, Handbook*. Burlington: Gulf Professional Publishing.
- [33] Bourgoyne Jr., A.T., Millheim, K.K., Chenevert, M.E. , & Young, Jr. F.S. (1986) *Applied Drilling Engineering*. Richardson: Society of Petroleum Engineers.
- [34] Freeman M.A. (2010) *An Introduction to Drilling Fluid – and Making Deep Holes*. MI-SWACO report.
- [35] Heald C.C. (2010). *Cameron Hydraulic Data: A Handy Reference on the Subject of Hydraulics, and Steam*. Boston: Ingersoll-Rand Company.
- [36] Matson H.D. (1998) *Weatherford Technical Data Handbook*. Houston: LP.
- [37] Brennen E.C. (1995). *Cavitation and Bubble Dynamics*. New York: Oxford University Press.
- [38] Lauterborn W. (1976). Numerical investigation of nonlinear oscillations of gas bubbles in liquids. *The Journal of the Acoustical Society of America* 59, (2), 283–293.
- [39] Shi W.T., Forsberg F. (1998). Acoustic detection of microbubble destruction in gaseous contrast agents. *The Journal of the Acoustical Society of America* 103, (5), 3002–3003.

Appendix A: Downhole vibration tools specifications

Tool	Inventor	Frequency, Hz	Amplitude of pulses, MPa	Pressure loss on the tool, MPa	Flow rate, gpm	Bit size, inch	Applied forces on the bit	Field test
Hydraulic pulsed cavitating jet generator	China University of Petroleum	up to 10	1.5 - 2.2	0.56 - 0.60	400 - 500	8.5	N/A	Several field tests at the depth range 1300 to 6100 m. ROP increase: 10 to 100%
High frequency cavitation hydrovibrator	Insitute of Technical Mechanics, Ukraine	100 - 10,000	2 - 3 times higher than inlet pressure	30 - 95% of the inlet pressure	10 to 50	1.4 - 3	Acceler.: 50g to 15,000g	Test on experimental drilling ground. ROP improvement: 60 to 70%
					20 - 110	3.6 - 5.9		
					40 - 200	6 - 9.8		
HydroPull	Tempress	8 to 12	7 to 11	2.5 - 5	42 - 66	1.69	5.8 - 8.9	Full scale tests were reported, but not the field test. Reported ROP improvement 33% to 200%
		10 to 17	7 to 11	2.5 - 12	66 - 105	2.12	7.5 - 12.5	
		6 to 12	6 to 9	2.2 - 3.5	105 - 145	2.88	9.8 - 14.2	
Agitator Tool	NOV	12 to 26	N/A	3.1 - 4.8	150 - 330	6	N/A	Field proven
Mud hammer	Novatek	10	Depends on flow rate, bit pressure drop and hammer mass	No significant pressure loss, flow loss up to 50%	Works with any flowrate (tested at 400 gpm)	8.5	Hammer impacts are function of BHP	Test at Terratek facilities reported ROP improvement from 10 to 100%, at pressure range 300 to 3000 psi

Appendix B: Prototype Drawings





Appendix C: Experimental Results

Test run #	Flow rate, gpm	Inlet pressure P1, psi	Outlet pressure P2, psi	Pressure drop, psi	P2/P1 ratio	Maximum acceleration n, g	Accelerometer frequency, Hz		Outlet pressure pulse frequency Po, Hz		Inlet pressure pulse frequency Pi, Hz
1	6	108	43	65	0.40	3.08	22	65	22	175	10
2	6	108	42	66	0.39	4.16	22	65	22	370	5
3	6	108	47	61	0.44	3.66	22	65	22	370	5
4	6	108	82	26	0.76	3.06	22	65	22	370	5
5	6	219	219	0	1.00	4.03	45	22	22	370	5
7	8	207	47	160	0.23	3.63	30	60	30	300	2
8	8	207	47	160	0.23	2.69	30	60	30	300	2
9	8	207	45	162	0.22	4.09	30	60	30	370	2
10	8	207	63	144	0.30	3.90	30	60	30	370	2
11	8	207	137	70	0.66	3.91	30	60	30	370	2
12	8	250	211	39	0.84	2.20	30	60	30	370	2
13	9.5	303	35	268	0.12	3.06	35	60	35	370	3
14	9.5	303	36	267	0.12	2.73	35	60	35	70	3

15	9.5	303	39	264	0.13	2.93	35	60	35	70	3
16	9.5	303	51	252	0.17	4.45	35	60	35	370	3
17	9.5	303	102	201	0.34	3.24	35	60	35	250	3
18	9.5	365	281	84	0.77	3.62	35	60	35	70	3
19	11	403	32	371	0.08	4.48	41	68	41	82	2
20	11	403	32	371	0.08	2.78	41	68	41	123	2
21	11	403	36	367	0.09	3.28	41	68	41	82	2
22	11	403	47	356	0.12	3.47	41	68	123	41	2
23	11	403	70	333	0.17	3.32	41	68	41	123	10
24	11	403	84	319	0.21	3.89	14	41	123	41	2 (14)
25	12	491	22	469	0.04	3.16	45	75 (90)	90	45	2
26	12	491	23	468	0.05	3.23	45	75 (90)	90	45	10
27	12	491	37	454	0.08	3.98	45	90	90	45	2
28	12	491	44	447	0.09	3.41	45	90	90	45	2
29	12	491	83	408	0.17	3.69	45	30 (90)	90	135	2
30	12	491	201	290	0.41	2.97	45	90	135	90	2
31	13.5	594	25	569	0.04	3.26	50	100	100	150	10
32	13.5	594	25	569	0.04	3.03	50	100	100	50	2

33	13.5	594	25	569	0.04	3.84	50	100	100	150	2
34	13.5	594	41	553	0.07	2.69	50	100	100	50	2
35	13.5	594	72	522	0.12	3.77	50	-	100	150	10
36	13.5	594	275	319	0.46	2.60	50	100	100	50	2
37	14.5	690	25	665	0.04	2.32	54	108	108	54	10
38	14.5	690	26	664	0.04	2.73	54	108	108	54	10
39	14.5	690	26	664	0.04	2.56	54	108	108	54	10
40	14.5	690	47	643	0.07	2.46	54	108 (40)	108	54	10
41	14.5	690	74	616	0.11	2.76	54	108	108	54	10
42	14.5	690	110	580	0.16	2.51	54	32	108	162	2
43	15.5	788	27	761	0.03	2.70	58	116	116	58	2
44	15.5	788	27	761	0.03	1.90	58	116	116	58	2
45	15.5	788	27	761	0.03	2.28	58	116	116	58	2
46	15.5	788	53	735	0.07	2.35	116	58	116	174	2
47	15.5	788	97	691	0.12	2.39	58	116	116	174	2
48	15.5	788	551	237	0.70	2.62	58	116	116	58	2

Appendix D: Confirmation Test Results

Test run #	Flow rate, gpm	Inlet pressure P1, psi	Outlet pressure P2, psi	Pressure drop, psi	P2/P1 ratio	Maximum acceleration, g	Accelerometer frequency, Hz		Outlet pressure pulse frequency Po, Hz		Inlet pressure pulse frequency Pi, Hz
1	9.5	298	45.8	252.2	0.15	2.54	35	-	35	420	2
2	9.5	296	47.8	248.2	0.16	2.01	35	-	35	70	2
3	9.5	297	51	246	0.17	3.65	35	-	35	70	2
4	9.5	297	56	241	0.19	3.62	35	-	35	420	2
5	9.5	298	63	235	0.21	2.86	35	-	35	70	2
6	9.5	297	70	227	0.24	3.09	35	-	35	70	2
7	9.5	298	85	213	0.29	3.47	35	-	35	370	2
8	9.5	297	104	193	0.35	2.50	35	-	35	70	2
9	9.5	297	122	175	0.41	3.01	35	-	35	70	2
10	9.5	297	161	136	0.54	2.68	35	-	35	70	2
11	9.5	305	227	78	0.74	2.89	35	-	35	70	2
12	9.5	340	270	70	0.79	2.52	35	-	35	70	2



